

# Embroidered antennas for communication systems

10

Z. Wang<sup>1</sup>, J.L. Volakis<sup>1</sup>, A. Kiourti<sup>1</sup>

<sup>1</sup>Ohio State University, Columbus, OH, USA

## 10.1 Introduction

Future personal wireless communication devices will require high data rates and reliable quality of service (QoS), regardless of the individuals' movements or the surrounding environment. Novel, flexible, lightweight, and wearable radio frequency (RF) electronics are capable of offering high-speed and reliable communications because they can be conformally installed at multiple locations within the garments (see Figure 10.1). Therefore, they can realize large on-body apertures to overcome size restrictions in handheld devices such as cell phones, personal digital assistants (PDAs), and others (Volakis et al., 2012; Zhang et al., 2012). Concurrently, such wearable RF electronics offer reliable wireless connectivity to a set of body-worn and multimode biosensors to enable low-cost and efficient day-to-day health monitoring (Salman et al., 2014). This is key to developing virtual point-of-care health centers that increase remote access to health care providers.

To realize efficient wearable RF functionalities without compromising comfort, highly flexible antennas and RF circuits are required that provide reliable RF performance and structural integrity for uninterrupted communications (Zhang et al., 2012). In this context, the recently introduced embroidered conductive textiles (Zhang et al., 2012; Wang et al., 2012a,b) are highly attractive. Specifically, they overcome traditional difficulties associated with cracking and deformation due to mechanical strain. Such textiles can be also printed onto low-loss and flexible polymer substrates to achieve additional structural integrity and RF performance for wearable RF electronics.

In this chapter, we describe the background and design rules for embroidered textile antennas. Characterization of the embroidered textiles at RF is provided, and several example textile designs are presented and tested for applications related to wearable RF electronics, medical monitoring, and radio frequency identification (RFID).

## 10.2 Background of textile antennas

Wearable electronics have been of interest for many years (Hamedi et al., 2007; Ouyang and Chappell, 2008; Wang et al., 2012b; Locher and Troster, 2008; Kim et al., 2008). A major challenge in designing wearable RF electronics is to achieve

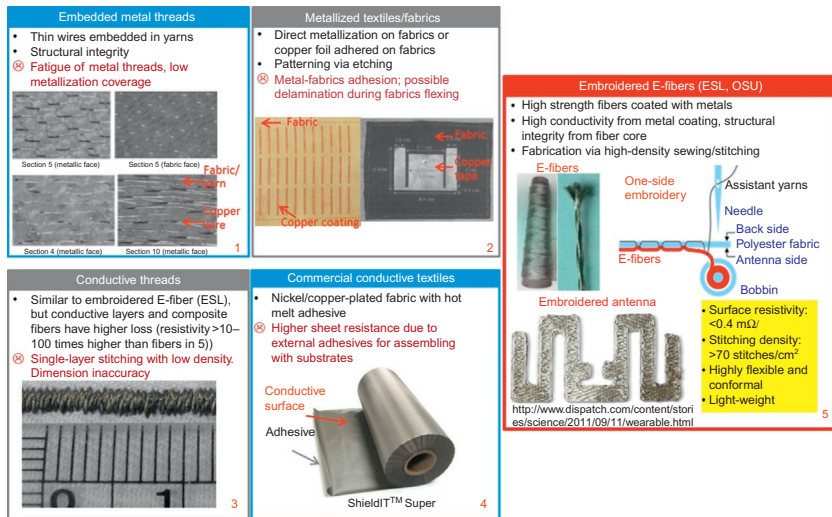


**Figure 10.1** Wearable RF electronics for high-speed communications.

excellent RF performance while the attire is concurrently comfortable and attractive (Zhang et al., 2012). To meet this requirement, embroidered flexible materials require a combination of high conductivity and mechanical strength (Ouyang and Chappell, 2008; Wang et al., 2012b; Locher and Troster, 2008; Morris et al., 2011). Conductive textiles have been reported to offer conformality, low-profile, and high conductivity for RF design applications (see Figure 10.2). For example, as described in Lilja et al. (2012), conductive antennas were fabricated by commercially available woven textiles on nonconductive substrates.

Among conductive textiles (see listing in Table 10.1), four categories can be distinguished: hybrid metal–textile fabrics, conductive yarn-based fabrics, embroidered conductive fabrics, and conductive ink-printed fabrics. As shown in Table 10.1, some conductive textiles experience metal fatigue after repetitive flexing, making them undesirable for wearable electronics. On the other hand, ink-jet-printed conductive textiles have low mechanical strength. Conductive textiles noted as (3), (4), and (5) in Table 10.1 exhibit good mechanical flexibility and conformality. However, they suffer from high conductor loss at RF.

Among the listed embroidered conductive textiles in Table 10.1, those noted as (6) exhibit the best combination of RF performance, mechanical strength, and load-bearing capability (Wang et al., 2012b; Toyobo Co., Ltd, 2005). In this chapter, we evaluate the RF characteristics of these embroidered E-fibers and their applications to antenna design. Of importance is that the materials used for the dielectric substrate of the embroidered textiles must also preserve the flexibility, integrity, and RF performance of the structure. In this chapter, we use polydimethylsiloxane (PDMS)



and its ceramic composites due to their advantages of tunable permittivity, low dielectric loss, and room temperature fabrication (Koulouridis et al., 2006; Wang et al., 2012b).

## 10.3 Design rules for embroidered antennas

### 10.3.1 Conductive textile threads

Silver-coated Amberstrand® fibers<sup>1</sup> were used to form the conductive textile surfaces for RF applications. These electronic fibers (E-fibers) are depicted in Figure 10.3a. They have a diameter of  $\sim 15 \mu\text{m}$  and are composed of a  $10\text{-}\mu\text{m}$  high-strength *p*-phenylene-2,6-benzobisoxazole (PBO) core (Toyobo Co., Ltd, 2005) and a  $2\text{--}3\text{-}\mu\text{m}$ -thick metallic coating (Wang et al., 2012b). The E-fibers exhibit a low direct current (DC) resistivity of  $0.8/\text{m}$ , coupled with excellent mechanical strength and flexibility. Measurement of the fiber conductivity over RF (0.1–20 GHz) showed that the effective conductivity of the E-fiber surface is  $\sigma = 3.5 \times 10^6 \text{ S/m}$  (Chung et al., 2012), which is comparable to that of copper. This high conductivity is critical to realizing passive RF devices using textiles.

<sup>1</sup> Syscom Advanced Materials, Inc.

**Table 10.1 Summary of conductive textiles in antenna and RF applications**

Category of conductive textiles	Conductive media	Characteristics	Reference
Hybrid metal-textile fabrics	(1) Embedded metallic threads (2) Metallized textiles (3) Commercial conductive textiles	Metal fatigue, high contact resistance Metallization rupture under bending High sheet resistance, extra loss due to adhesives	Ouyang and Chappell (2008) Bashir et al. (2009) Vallozzi et al. (2009)
Conductive yarn-based fabrics	(4) Conductive carbon fiber-braided fabrics	High resistivity and loss	Mehdipour et al. (2010)
Embroidered conductive fabrics	(5) Conductive threads  (6) Metal-coated polymer fibers (E-fibers)	High conductor loss due to low-quality metallization  Low conductor loss, excellent mechanical strength	Locher and Troster (2008) and Kim et al. (2008) Toyobo Co., Ltd (2005)
Conductive ink-printed fabrics	(7) Ink-jet-printed textiles	Low mechanical strength, ink surface rupture under flexing and stretching	Li et al. (2012) and Zhou et al. (2010)

### 10.3.2 Embroidered process of conductive textile surfaces

A unique embroidery process was adopted using a computerized sewing machine. As shown in Figure 10.4, antenna and circuit designs were translated into embroidery patterns, followed by digitization of the stitching locations. An assistant yarn is used to precisely and firmly couch the E-fibers onto one side of the textile surface (Wang et al., 2012b). As such, possible abrasion damage of the metallic fiber coatings is avoided. Prototype E-fiber antennas (see Figure 10.3) were shown to have an excellent mechanical flexibility, allowing for conformal and even 3D adaptations of their surface. To explore the E-fibers' viability in constructing multilayer RF circuits, a process for multilayer, microstrip circuit structure was also developed using via pins made by E-fibers (Wang et al., 2012b).

As can be understood, it is important to ensure maximum conductivity for the textile surfaces. To do so, the aforementioned embroidery process was tailored to realize double textile layers; that is, a second layer was embroidered on top of the first. In this way, possible physical discontinuities and thread gaps were minimized. We found that the latter were always less than  $\lambda/20$ , with  $\lambda$  being the free-space wavelength at the

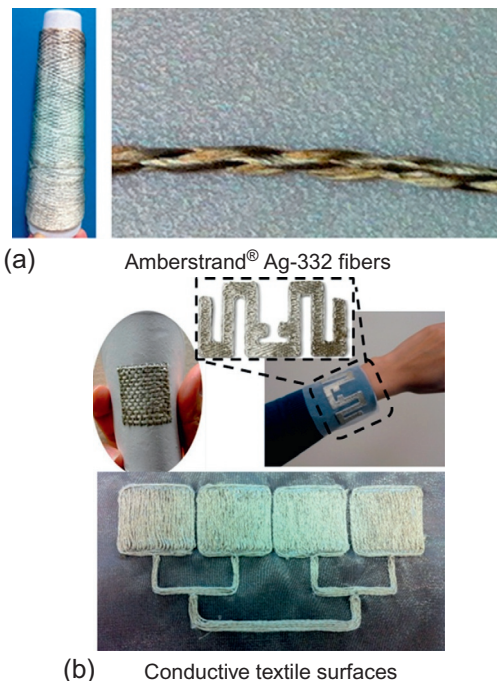


**Figure 10.3** (a) Multiple-strand conductive fibers and (b) their associated conductive textile surfaces.

From [Wang et al. \(2014\)](#), ©2014 IEEE.

operation frequency. This accuracy is a remarkable achievement and critical to realizing high-performance antennas and RF circuits.

### 10.3.3 *Integration of embroidered textile surfaces onto polymer substrates*

The aforementioned embroidered textiles were integrated on a low-loss and highly flexible polymer substrate. We employed PDMS as our substrate due to its mechanical flexibility and stretchability, inherent chemical stability, and water resistance ([Koulouridis et al., 2006](#)). As demonstrated in [Wang et al. \(2012b\)](#), the resultant PDMS composite had a dielectric constant of  $\epsilon_r = 3.0$  and a low-loss tangent of  $\tan\delta < 0.02$ . Another advantage of PDMS is that its permittivity can be increased from  $\epsilon_r = 3.0 - 13.0$  by dispersing ceramic powder into the PDMS matrix ([Koulouridis et al., 2006](#)).

The process of integrating the textile surfaces onto a polymer substrate is depicted in [Figure 10.5](#) for a microstrip transmission line (TL) structure ([Zhang et al., 2012](#)). Embroidered TLs and ground planes were first laminated with PDMS. Then, the two PDMS sides were joined using an extra-thin layer of uncured PDMS ([Wang et al., 2012b](#)).

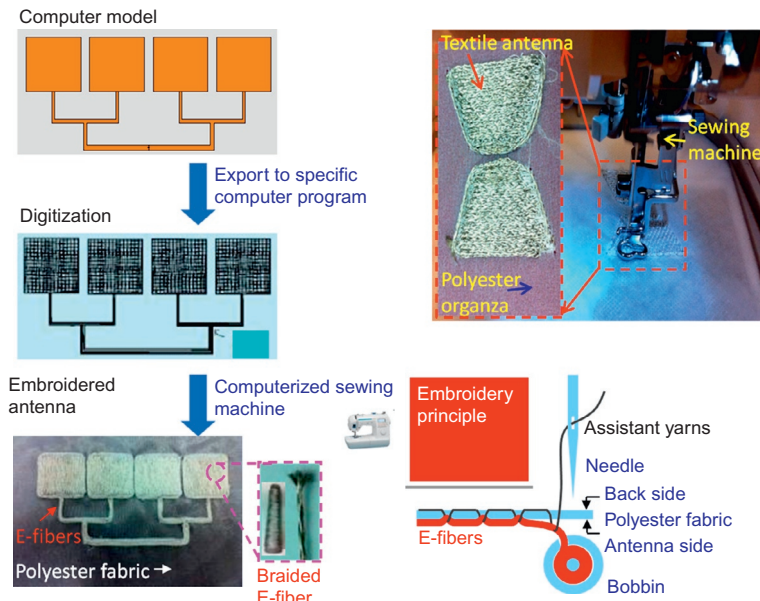


**Figure 10.4** Fabrication of embroidered textile surfaces.

From [Wang et al. \(2012b\)](#), ©2012 IEEE.

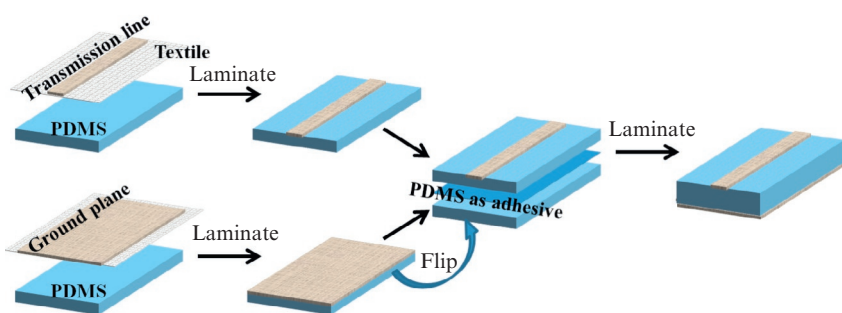


**Figure 10.5** Fabrication of textile surface onto polymer substrates.

From [Zhang et al. \(2012\)](#), ©2012 IEEE.

Several RF devices were fabricated (see [Figure 10.6](#)) using the above process. They include a 50-microstrip line, a patch antenna, a 4-by-1 antenna array with feed network, and a spiral antenna. We note that all these structures remained intact after repetitive flexing and stretching.

An example of assembling multilayer RF devices is depicted in [Figure 10.7](#). The design consists of two PDMS layers, each having an embroidered TL on the surface. To fabricate the two-layer structure, two TLs were joined using an extra-thin layer of PDMS. A via was then created by pushing an E-fiber string through the polymer using

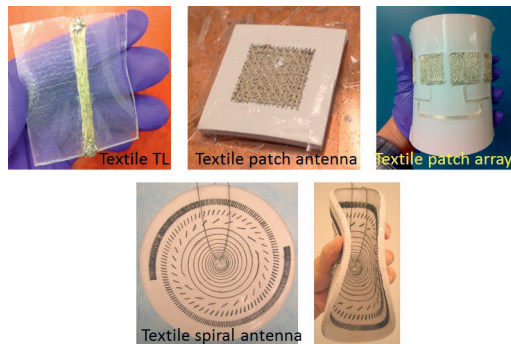


**Figure 10.6** Various fabricated RF patterns using textiles on PDMS substrate: textile transmission line, patch antennas, and spiral antenna.

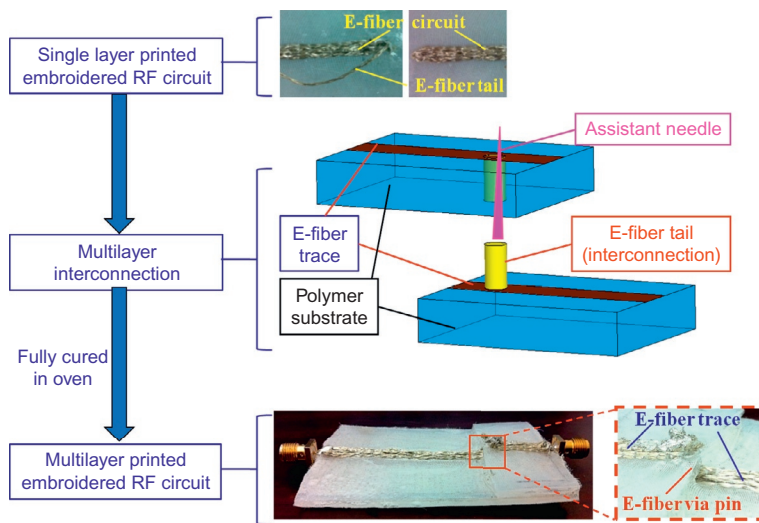


**Figure 10.7** Fabrication multilayer textile-based RF circuits.  
From [Wang et al. \(2012b\)](#), ©2012 IEEE.

a syringe or needle. We remark that this double-layer embroidered RF circuit retained very high flexibility and did not deteriorate in RF performance after repeated flexing.

## 10.4 Characterizations of embroidered conductive textiles at radio frequencies

### 10.4.1 Losses in conductive textiles at radio frequencies

#### 10.4.1.1 Embroidered textile microstrip lines

The RF performance of the embroidered E-fiber surfaces was tested using a 5-cm-long  $50\ \Omega$  microstrip TL ([Wang et al., 2012b](#)). As depicted in [Figure 10.8](#), three samples were fabricated on PDMS substrates. The electrical loss of the textiles was then

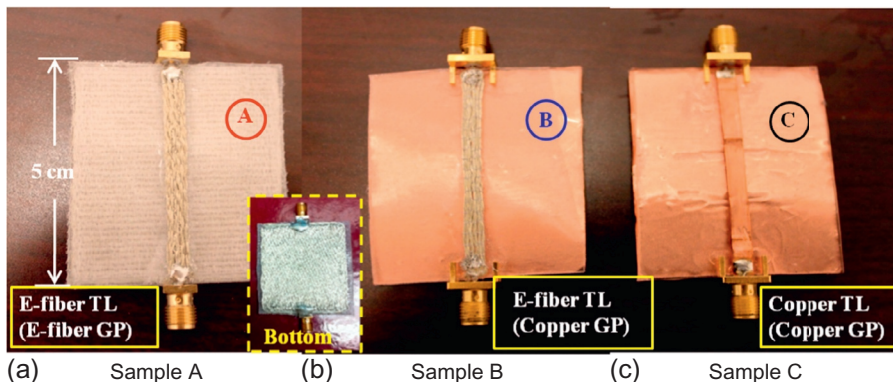


**Figure 10.8** Three single-layer microstrip line samples: (a) E-fiber TL with E-fiber ground plane, (b) E-fiber TL with copper ground plane, and (c) copper TL with copper ground plane. From Wang et al. (2012b), ©2012 IEEE.

evaluated by measuring the *S*-parameters with a 2-port Agilent N5230A network analyzer. As shown in Figure 10.9, the E-fiber TL with E-fiber ground plane (sample A in Figure 10.8) had an insertion loss of 0.2 dB/cm up to 4 GHz, which is only 0.07 dB/cm higher than that of the all-copper TL structure (sample C in Figure 10.8). Good impedance matching up to 5 GHz is also exhibited.

The above results demonstrate the remarkably high conductivity of the flexible embroidered textiles and low loss of the flexible PDMS substrate at RF. As expected, loss increases with frequency. But of more importance is the fact that the overall loss of E-fibers was very low. We remark that the embroidered E-fiber textiles sustained their RF performance and structural integrity after repetitive flexing (Wang et al., 2012b). These characteristics are highly attractive for wearable RF applications.

To better demonstrate the flexibility of our E-fibers on polymer, we also considered a pair of TL printed on different PDMS layers and connected them through vias. Figure 10.10 shows the fabricated double-layer PDMS in flat and flexed forms. For comparison, a double-layer copper TL was also fabricated on the same PDMS. Figure 10.11 gives the measured S21 for the 2-layer TL, indicating a value of less than 0.34 dB/cm up to 4 GHz. This is only 0.2 dB/cm higher than that of the copper sample. Therefore, both single- and double-layer embroidered E-fiber TLs delivered satisfactory RF performance and excellent mechanical properties (structural flexibility and integrity).

#### 10.4.1.2 Losses in conductive textiles

To extract explicit propagation constants along the TLs, three E-fiber microstrip lines were fabricated and measured (see Figure 10.12; Zhang et al., 2012). As described in Wang et al. (2012b), the fibers were first embroidered to form the textile TLs, followed by their integration onto the polymer substrates ( $\epsilon_r=3$ ,  $\tan \delta < 0.01$ ). The E-fiber TLs and their copper counterparts were measured from 30 MHz to 6 GHz,

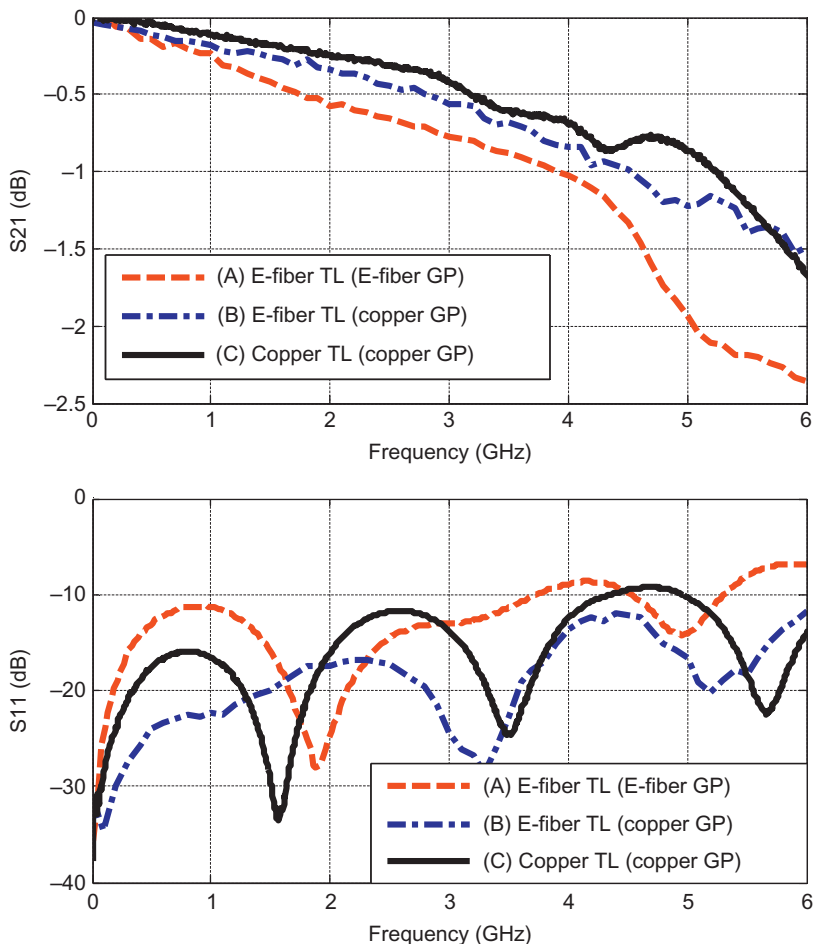


**Figure 10.9** Measured S-parameters of the three single-layer TL samples.  
From Wang et al. (2012b), ©2012 IEEE.

and the reflection coefficient ( $S_{11}$ ) and insertion loss ( $S_{21}$ ) are shown in Figure 10.13. As shown in Figure 10.13d, the measured  $S_{11}$  of E-fiber TLs was less than  $-10$  dB, indicating good impedance match across the entire frequency range.

We proceeded to extract the attenuation loss of the E-fibers by calculating the loss-per-unit length from the measured  $S_{21}$ . Three E-fiber TLs of different lengths ( $l_1$ ,  $l_2$ ,  $l_3$ ) were fabricated to accurately de-embed the measured results (Mangan et al., 2006) and to extract the actual attenuation constants,  $\alpha$  (Pozar, 2004). As is well known, the TL de-embedding technique is a cost-effective method to extract the RF characteristics of the TLs. Meanwhile, three copper TLs of the same lengths are also used as a reference.

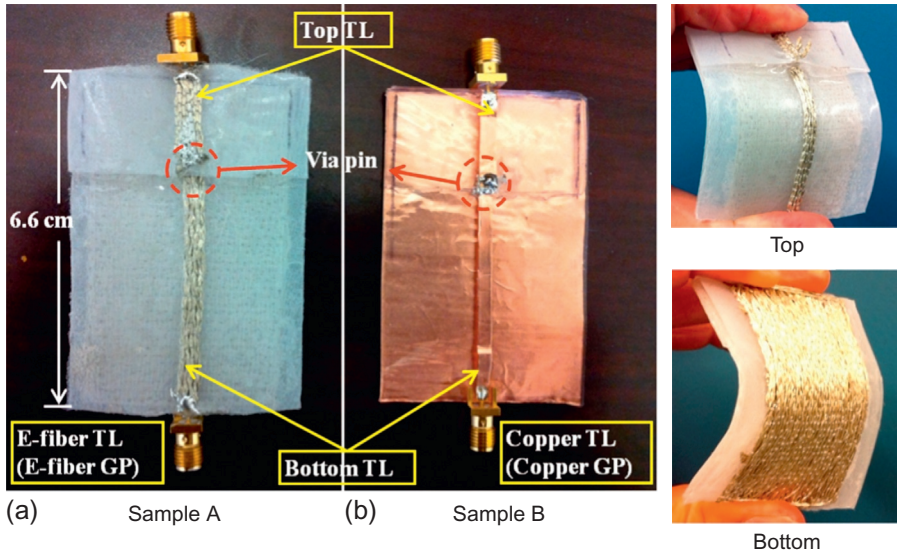


**Figure 10.10** Double-layer microstrip transmission lines fabricated of (a) E-fibers and (b) copper.

From Wang et al. (2012b), ©2012 IEEE.

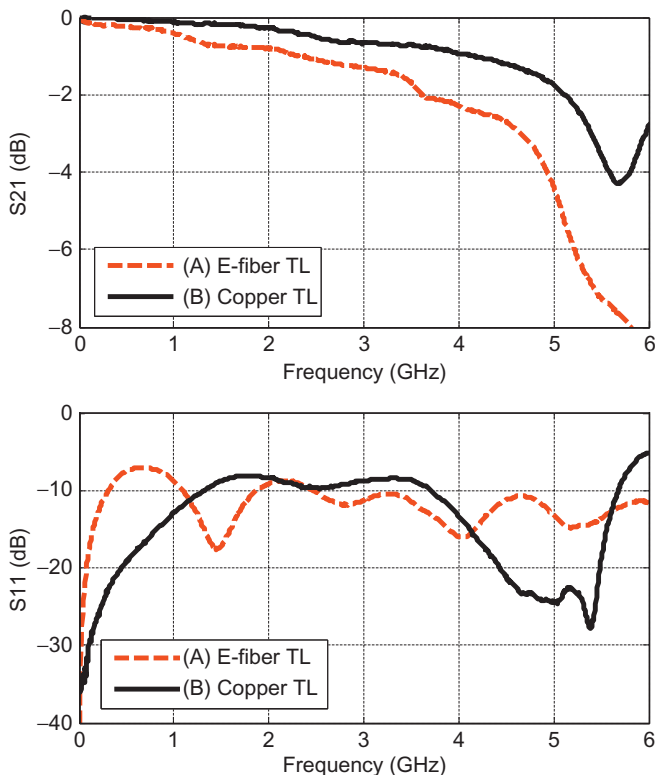


**Figure 10.11** Measured S-parameters of the double-layer TL samples.

From Wang et al. (2012b), ©2012 IEEE.

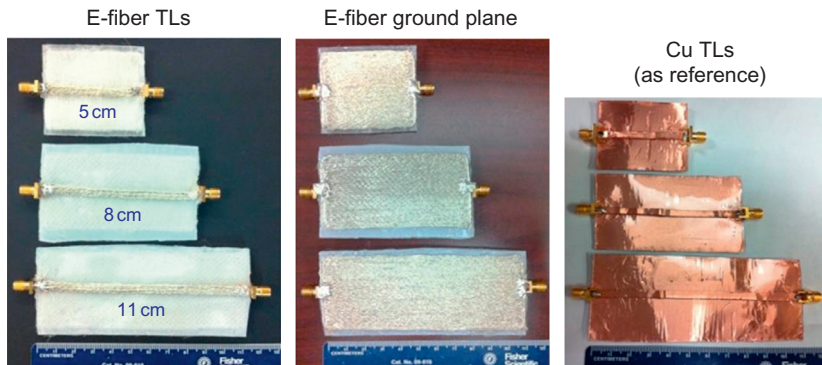


**Figure 10.12** Fabricated textile TLs and reference copper TLs.

From [Zhang et al. \(2012\)](#), ©2012 IEEE.

The extracted attenuation constants for the E-fiber and copper TLs are shown in [Figure 10.14](#). As we see,  $\alpha_{\text{E-fiber}}$  is slightly higher than  $\alpha_{\text{copper}}$  from 30 MHz up to 4 GHz. At 1 GHz,  $\alpha_{\text{E-fiber}} = 0.14 \text{ dB/cm}$ , which is only 0.1 dB/cm higher than that of copper. As the frequency goes higher,  $\alpha_{\text{E-fiber}}$  is increased to  $\alpha_{\text{E-fiber}} = 0.19 \text{ dB/cm}$  at 3 GHz and  $\alpha_{\text{E-fiber}} = 0.27 \text{ dB/cm}$  at 4 GHz, which is 0.15 dB/cm and 0.17 dB/cm higher than their copper counterparts, respectively. We observe that at higher frequencies, the attenuation in the textile TLs increases due to conductor losses caused by surface roughness and imperfect metallization of the E-fibers. Nevertheless, the overall loss-per-unit length in E-fibers is small, making them an efficient conductor for RF designs.

### 10.4.2 Influence of embroidery density on textile's insertion loss

The macrostructure of the E-fiber and the aforementioned embroidery process result in air gaps between the E-fiber threads. As a result, the textile surface conductivity is reduced. An effective way to reduce the loss is to increase the density of the conductive media ([Pozar, 2004](#)). This can be realized by increasing the embroidering density or by using higher density fibers. Below, we investigate the influence of fiber and stitching density on insertion loss (S21). As shown in [Figure 10.15a](#), a 5-cm embroidered microstrip TL was used, and several types of braided E-fibers were formed by changing the number of strands used to embroider the surface (see [Table 10.2](#)).

#### 10.4.2.1 Stitching density

Generally speaking, denser embroidery is preferred, as it reduces potential physical discontinuities in the textile surfaces. Concurrently, conductivity is increased. However, in practice, denser embroidery is more challenging to carry out and may result in sewing needle breakage. Therefore, the embroidery density is optimized to achieve a compromise between high-quality embroidery and feasible fabrication. As shown in [Table 10.2](#), a low loss of 0.2 dB in insertion loss was observed at 3 GHz for a 664-thread E-fiber TL (sample E) when the embroidery density increased from 1.6

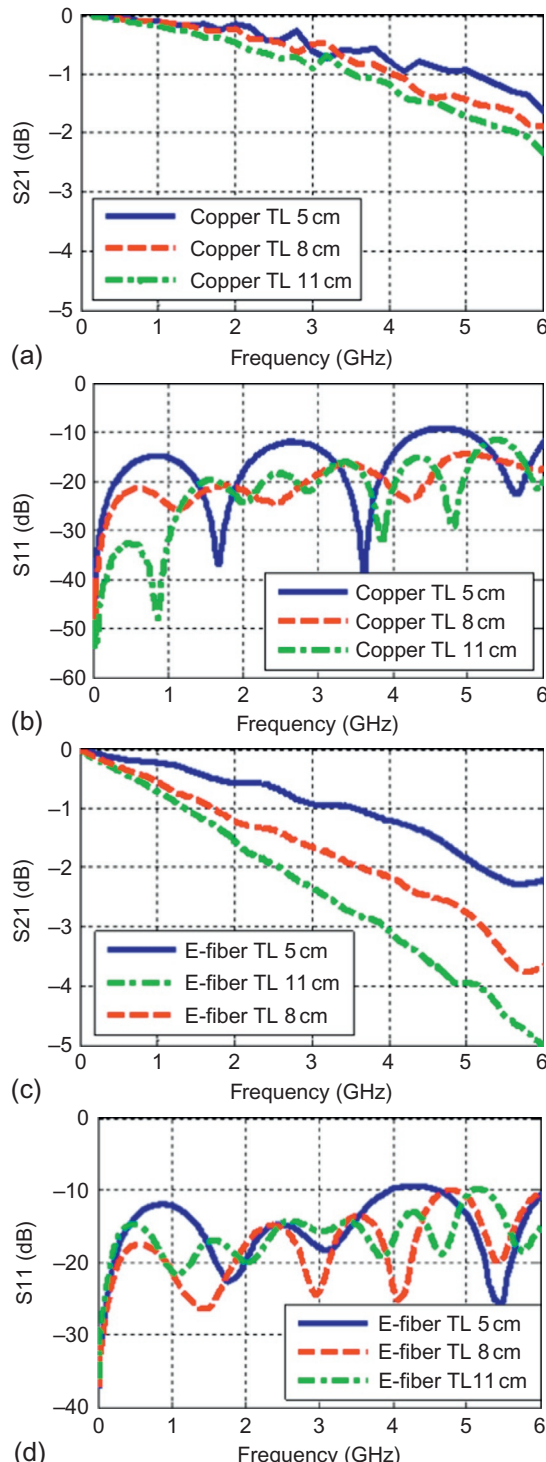


**Figure 10.13** Measured S-parameters of textile and copper TLs: (a) copper TL—S<sub>21</sub>, (b) copper TL—S<sub>11</sub>, (c) E-fiber TL—S<sub>21</sub>, and (d) E-fiber TL—S<sub>11</sub>.

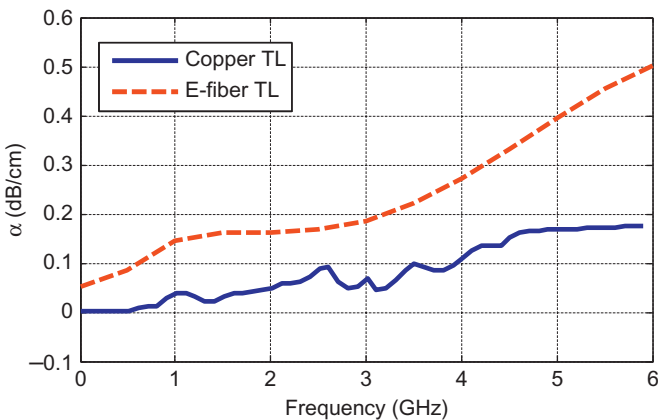


**Figure 10.14** Extracted attenuation constant of the E-fiber and copper TLs using the de-embedding method.

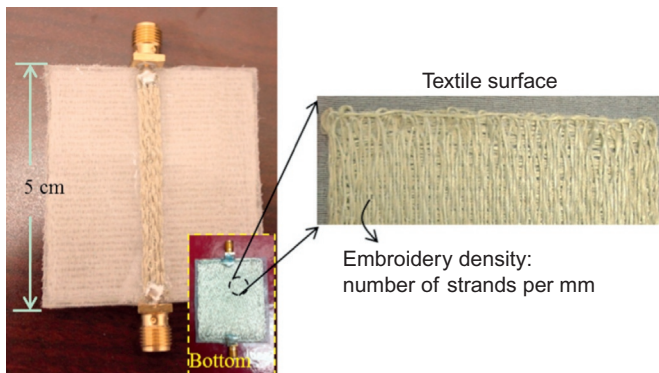


**Figure 10.15** Sample of embroidered E-fiber TL.

to 2.0 strands/mm. However, further increasing the embroidery density to 2.7 strands/mm does not result in much reduction of loss. This indicates that the effective conductivity achieved a plateau at around 2.0 strands/mm.

#### 10.4.2.2 Fiber density

Further, we examine the performance of TL samples embroidered with E-fibers of different thread densities. As depicted in Table 10.2, E-fiber TLs made of denser E-fibers clearly exhibited lower loss. That is, for TLs having the same stitching patterns, heavier fibers resulted in denser surface coverage (much like thicker carpets) and higher conductivity. We also observe that the loss for TL samples made by

**Table 10.2 Impacts from embroidery parameters**

Sample	Conductive material		Embroidery density (strand/mm)	5 cm TL loss at 3 GHz (dB/cm)
	Transmission line	Ground plane		
A	166-Thread E-fibers	Copper	4.0	0.15
B	166-Thread E-fibers	166-Thread E-fibers	4.0	0.28
C	332-Thread E-fibers	332-Thread E-fibers	3.0	0.20
D	664-Thread E-fibers	664-Thread E-fibers	1.6	0.23
E	664-Thread E-fibers	664-Thread E-fibers	2.0	0.20
F	664-Thread E-fibers	664-Thread E-fibers	2.7	0.19
Reference	Copper	Copper	–	0.08

332-thread and 664-thread E-fibers is approximately the same, even though the 664-thread E-fiber's weight was doubled. This indicates that the conductive fiber density approached the limit of our current achievable conductivity in this frequency range. E-fibers formed of more than 664 strands were difficult to handle due to sewing needle breakage. Concurrently, they are likely to lead to geometrical inaccuracies. Therefore, the 664-thread E-fibers were found to be the most suited for the proposed embroidery process.

#### 10.4.2.3 Protection of E-fiber textile surface

The conductive fibers have silver coatings of  $\sim 2 \mu\text{m}$  in thickness, which may suffer from corrosion and weathering. This, in turn, decreases their surface conductivity. As shown in [Figure 10.16b](#), without any protection, the loss of a 5-cm E-fiber TL increased up to 0.3 dB after a year, mainly due to silver corrosion. Therefore, in order to maintain the RF performance of E-fiber structures, it is critical to encapsulate the E-fiber surface with a low-loss thin film of polymer. As seen in [Figure 10.16](#), two polymer-based thin films, namely polyurethane (PU) ( $\epsilon_r=3.2$ ,  $\tan \delta=0.02$ ) and PDMS ( $\epsilon_r=3.0$ ,  $\tan \delta=0.01$ ), are employed. We note that both polymer films are mechanically compatible with the flexible and conformal E-fiber surfaces. In this study, both PDMS and PU films were fabricated and tightly laminated around the 5 cm E-fiber TLs, as shown in [Figure 10.16a](#). The transmission coefficient (S21) of the three E-fiber TL samples is shown in [Figure 10.16c](#). We verified that

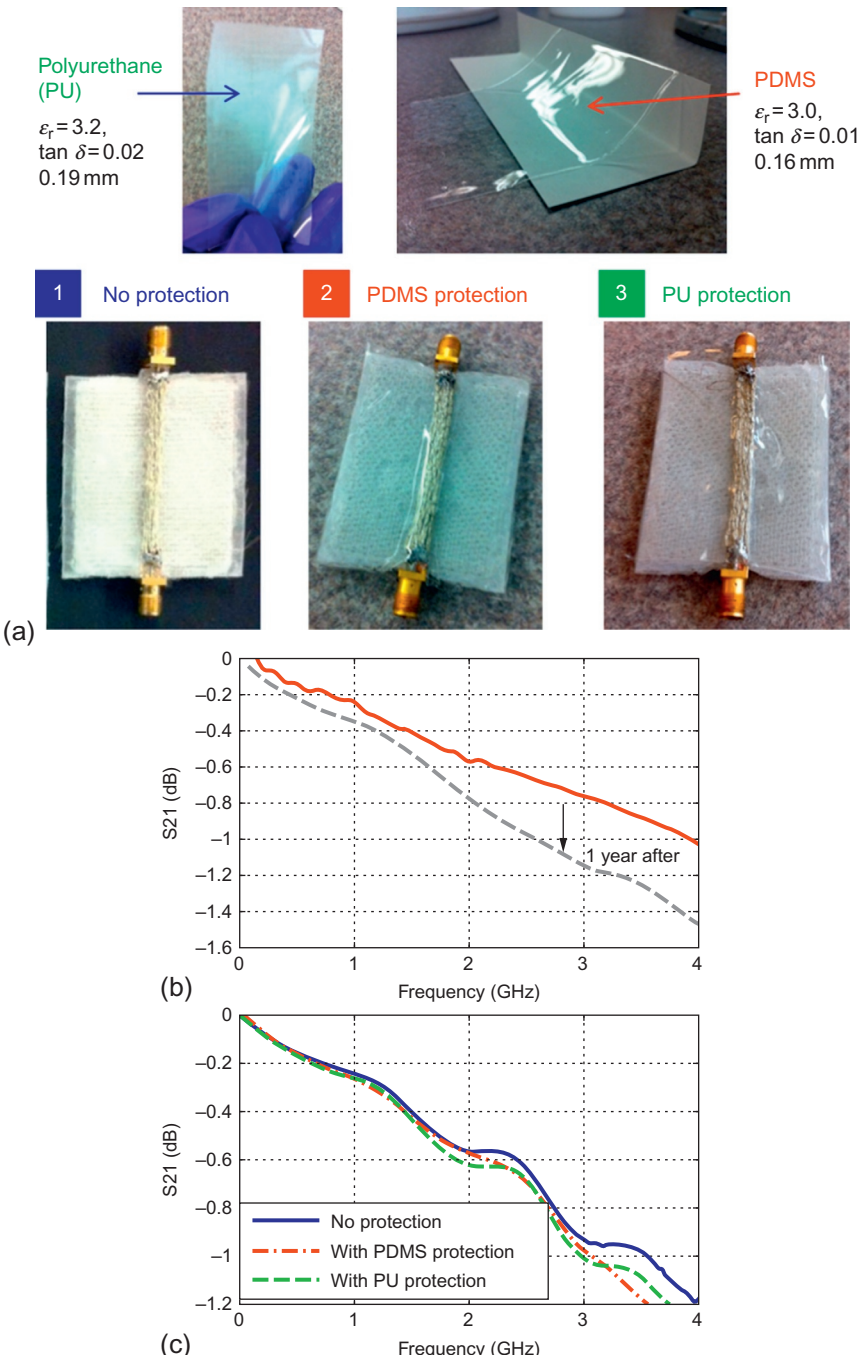


**Figure 10.16** (a) E-fiber TL with polymer encapsulation to prevent weathering and corrosion of conductive textile surface; (b) increased loss in a 5-cm E-fiber TL after a year with no protection of textile surface; and (c) comparison of S21 of unprotected and encapsulated 5-cm E-fiber TLs.

hardly any loss was introduced by the thin protection films. In future applications, PU will be preferred due to its higher mechanical strength and lower water permeability.

### **10.4.3 RF performance of embroidered textile antennas**

To demonstrate the RF performance of textile antennas, sample patch antennas are fabricated for experimental verification on both planar and curved surfaces (Wang et al., 2012b). Measurements showed that the RF performance of the E-fiber patch antennas on polymer substrate is as good as that of their copper counterparts.

#### **10.4.3.1 Embroidered textile patch antenna**

First, an embroidered textile patch antenna was fabricated on a polymer substrate ( $\epsilon_r=4.2$  and  $\tan\delta=0.01$ ). Next, the antenna was measured on planar and cylindrical surfaces (see Figure 10.17). As shown in Figure 10.17a, the measured resonance frequency of the planar textile patch antenna was 2.2 GHz, agreeing with that of its simulated copper counterpart. The measured realized gain was 5.6 dBi, which is only 0.3 dB lower than that of the copper patch antenna. The measured patterns were also in agreement with simulations. We further note that this remarkable RF performance of the textile antenna does not degrade after repetitive flexing (more than 20 times).

To further evaluate the RF performance of the E-fiber antenna, the latter was mounted on a metallic cylinder (diameter=80 mm). As shown in Figure 10.17b, the measured reflection coefficient and radiation patterns of the textile patch antenna were in good agreement with the simulations of the equivalent copper patch antenna. The realized gain was only 1 dB lower than simulation. Further, as compared to the flat configuration, the textile antenna had a lower resonance frequency of 2.06 GHz and a reduced gain of 3.0 dB. The frequency detuning is due to the 13% elongation of the patch dimension in the H-plane (Wang et al., 2012b). However, the gain reduction is primarily because of the curvature and higher resistance of the textile's surface. The latter was due to the stretching of the E-fiber threads. Nevertheless, these results clearly demonstrate the remarkable RF and mechanical performance of the E-fiber antenna.

#### **10.4.3.2 Embroidered textile antenna array**

A 4-by-1 textile antenna array was next fabricated and tested (see Figure 10.18). As shown in Figure 10.18a, the textile antenna array has a resonance frequency of 2.31 GHz and a realized gain of 7.0 dBi. The resonance frequency agrees well with simulation and measurement of its copper counterpart. Also, the realized gain of the textile array was only 0.6 dB lower than the simulated and measured gain of the copper array. The slight discrepancy in the resonance frequency between the three array samples in Figure 10.18a was likely due to geometrical inaccuracies of the fabricated textile array.

The performance of the textile array mounted on a curved surface was measured next. For comparison, an equivalent copper array was also fabricated (see

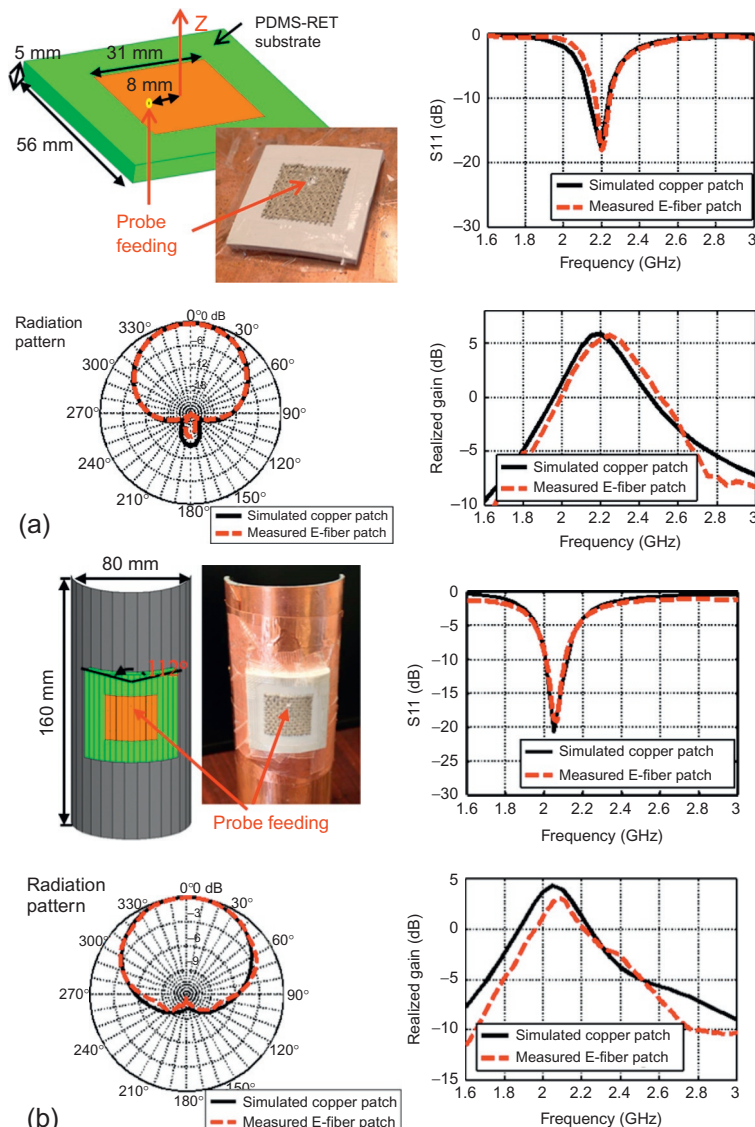


**Figure 10.17** Textile patch antenna and its RF performances (a) on a planar surface and (b) mounted on a cylindrical surface.

From Wang et al. (2012b), ©2012 IEEE.

**Figure 10.18b)**. The measured performance of the textile patch array was in good agreement with that of the copper array and the corresponding simulation. Particularly, the realized gain of the E-fiber array was 4.6 dBi, 1 dB lower than that of the copper array. We note that the increased spacing between the patch elements during bending led to the difference between the radiation patterns of the flat and curved

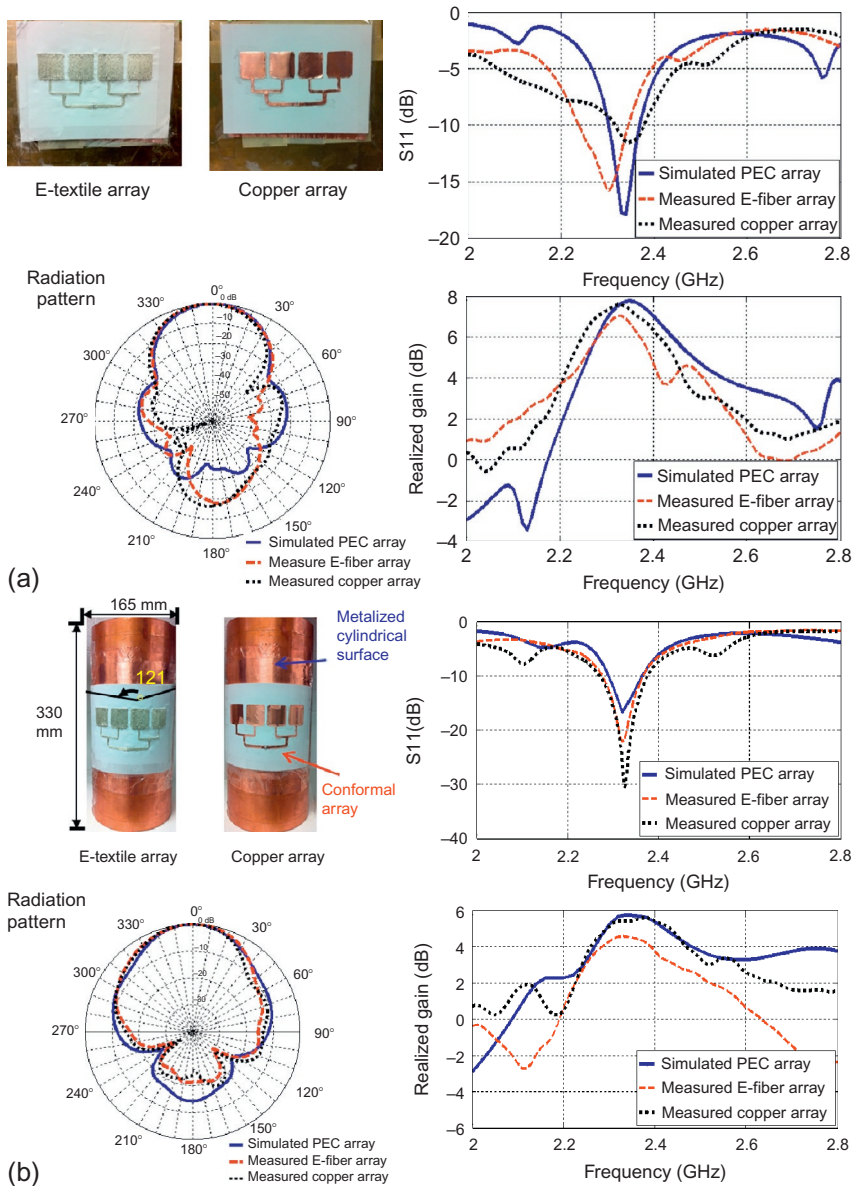


**Figure 10.18** Textile antenna array and its RF performance (a) on a planar surface and (b) mounted on a cylindrical surface.

From Wang et al. (2012b), ©2012 IEEE.

configurations. Measurement results of the antenna arrays as well as the single patch antenna are summarized in Table 10.3.

In summary, we remark that embroidered textile antennas indeed demonstrated no compromise on antenna performance and efficiency. This is in addition to their

**Table 10.3 Summary of embroidered antenna performance**

	Conductor	Planar surface		Curvilinear surface	
		$f_{\text{resonant}}$ (GHz)	Realized gain (dBi)	$f_{\text{resonant}}$ (GHz)	Realized gain (dBi)
Patch antenna	Simulated Cu	2.21	5.9	2.05	4.3
	Textile	2.20	5.6	2.06	3.0
Antenna array	Simulated Cu	2.36	7.6	2.32	5.7
	Textile	2.31	7.0	2.33	4.6

From Wang et al. (2012b), ©2012 IEEE.

mechanical flexibility. Such embroidered antennas are also easy to stitch onto polymer substrates for further integration onto any shaped platform, such as clothing (Wang et al., 2013a, 2014) and vehicle frames (Wang et al., 2012b).

## 10.5 Applications of embroidered antennas

### 10.5.1 Embroidered textile antennas for body-worn UHF communications

A meandered flare dipole antenna was designed to operate at a 600 MHz ultra-high frequency (UHF) band. As shown in Figure 10.19a, this textile antenna is flexible on both concave and convex surfaces, making it promising for wearable communications. Both the textile antenna and its copper counterpart were measured in free space. As demonstrated in Figure 10.19b, the textile antenna resonated at 610 MHz, which is in agreement with that of its copper counterpart and simulation. We found that the textile dipole's realized gain was 1 dB, which is 0.8 dB lower than that of copper (see Figure 10.19c). This was likely due to the conductor loss on the E-fiber surface. Nevertheless, the E-fiber textile antenna provided satisfactory RF performance, along with mechanical benefits, making it feasible for UHF body-worn communications.

Subsequently, the antenna performance was studied in the presence of a human-shaped phantom, as shown in Figure 10.20. The mannequin was filled with tissue-emulating liquid composed of water, sugar, and salt, which had a relative dielectric constant of  $\epsilon_r=56.7$  and conductivity of  $\tan\delta=0.94$  S/m (Wang et al., 2012b). Figure 10.20 shows the azimuth radiation patterns of the textile antenna when it was placed in the front ( $0^\circ$ ) and back torso ( $180^\circ$ ) of the mannequin. As can be seen, the performance of the body-worn textile antenna matched well with that of its copper counterpart, with a measured realized gain of  $-4$  dB. Importantly, the use of multiple body-worn textile antennas can lead to omnidirectional signal coverage, making it very suitable for robust wearable communications (Lee et al., 2011).

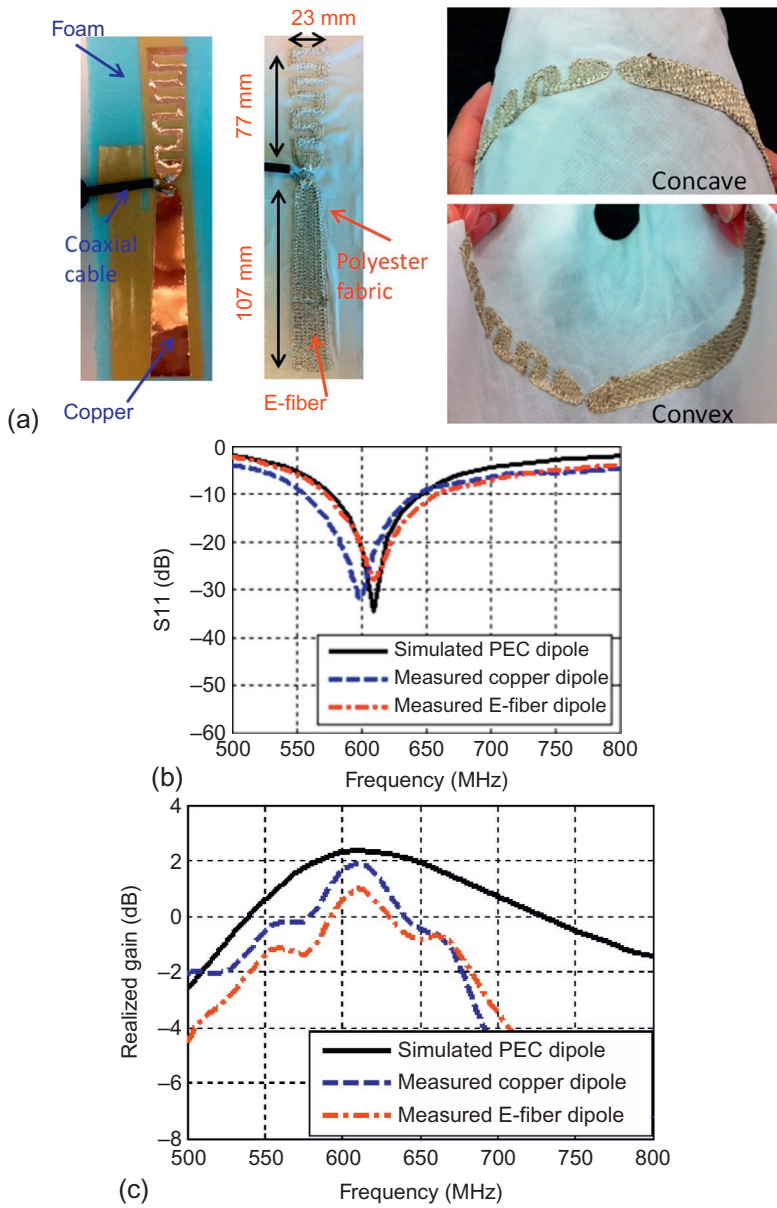


**Figure 10.19** (a) Flexible embroidered textile dipole antenna and its copper counterpart, (b) measured S11, and (c) measured realized gain in free space.

We also evaluated the E-fiber antenna's RF performance when the textile antenna was embroidered on a polyester scarf (see Figure 10.21a). The textile antenna's performance was measured outdoors in windy weather (Wang et al., 2013a), as shown in Figure 10.21a, to ensure repeatable and reliable performance even when the scarf

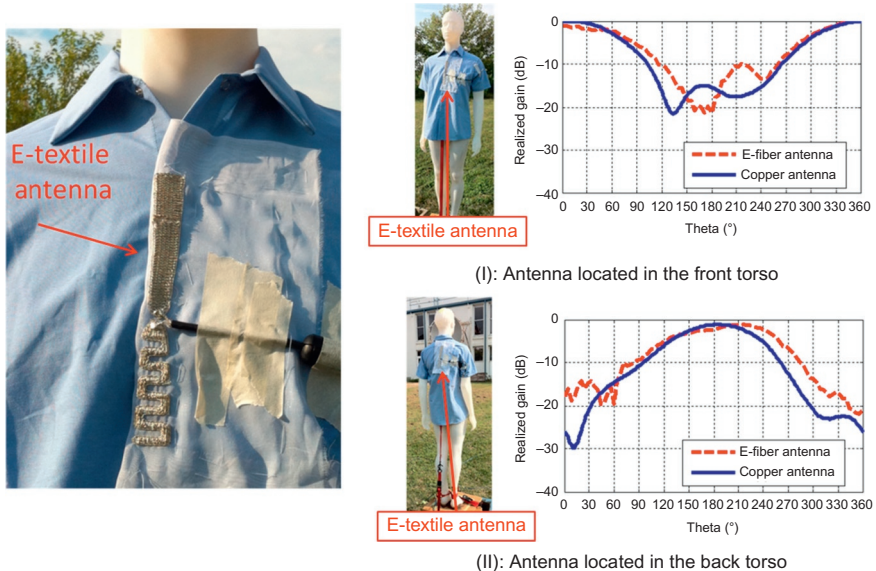


**Figure 10.20** Wearable textile antenna sewn on a cotton shirt, and measured radiation patterns of the textile and copper antennas at 600 MHz for different on-body locations (Wang et al., 2013a).

moves in many positions. As shown in Figure 10.21, high gain was achieved when the antenna was embroidered on the scarf, compared to the case where the antenna was fixed on the phantom torso. This was because the scarf was blown far from the body, implying less influence from the lossy tissue.

Polarization mismatch was, of course, unavoidable when the textile antenna was on the scarf. Because of the scarf's continuous movement, a statistical analysis of the antenna performance was carried out to investigate its reliability. As seen in Figure 10.21, we found a 90% probability of the detected gains being over  $> -23$  dB for all five scarf-wearing cases (Wang et al., 2013a). We note that the textile antenna had a gain of  $-20$  dB when placed in front of the torso and  $-22$  dB gain when placed at the back of the torso.

## 10.5.2 Embroidered multiband antenna for body-worn GSM/PCS/WLAN communications

### 10.5.2.1 Embroidered multiband textile antenna design

In this section, we designed a flexible multiband antenna based on the aforementioned embroidered textiles. The proposed antenna operates at Global System for Mobile Communications (GSM 850/900 MHz), Personal Communications Service (PCS 1800/1900 MHz), and Wireless Local Area Network (WLAN 2450 MHz) bands. As demonstrated in Wang et al. (2014), an important aspect of this antenna is the loaded loop,

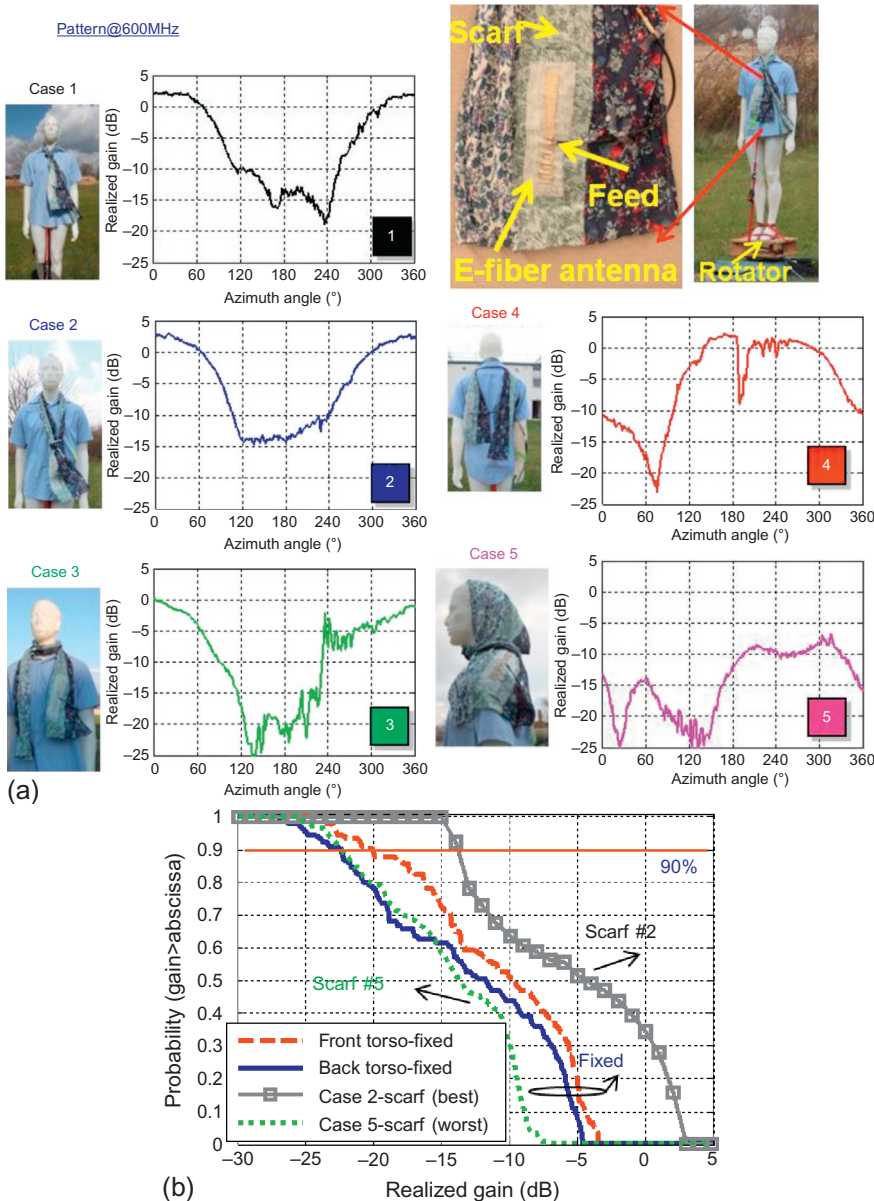


**Figure 10.21** Measured radiation pattern of textile dipole on a scarf in five different styles and at different on-body locations (Wang et al., 2013a): (a) measured pattern and (b) statistical analysis.

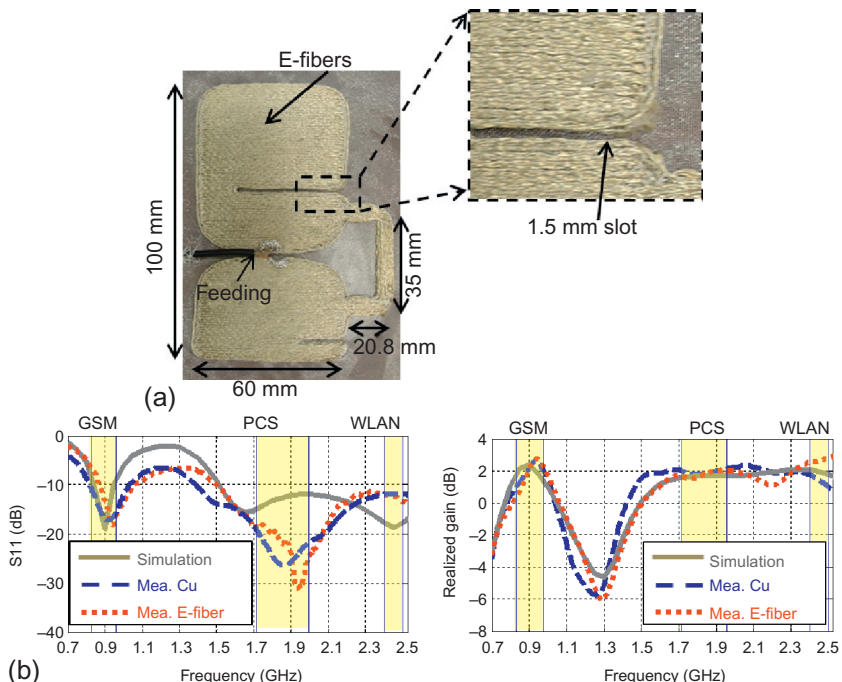


**Figure 10.22** (a) Embroidered multiband textile antenna using E-fibers, and measured and simulated RF performance of the textile antenna in free space: (b)  $S_{11}$ , (c) realized gain, and (d) radiation patterns.

From Wang et al. (2014), ©2014 IEEE.

critical for achieving a good impedance match at all three frequency bands. This multiband antenna was fabricated by embroidering E-fiber textiles with a fabrication precision of 0.5 mm, which is important to ensure accuracy in embroidering the slots of the design. As a reference, a copper version of the antenna was also fabricated. The fabricated textile antenna is first measured in free space. As shown in Figure 10.22, the textile antenna exhibited good impedance matching ( $S_{11} < -10$  dB) over all three frequency bands. Notably, it achieved a good gain of 2 dBi in all three frequency bands, a necessity to ensure reliable communication. In addition, the measured radiation patterns shown in Figure 10.23 confirmed the expected omnidirectional radiation performance. Also, the textile antenna's reflection coefficient ( $S_{11}$ ), realized gain and patterns were shown to be in good agreement with simulations and measurements of its copper counterpart. This confirmed the feasibility of E-fiber textile antennas.

### 10.5.2.2 Influence of the human body on antenna performance

The presence of the human body affects the performance of on-body antennas due to the high permittivity and loss of the biological tissues (Lee et al., 2011; Wang et al., 2014). Major effects include detuning of the antenna's resonance frequency, and radiation shadowing.

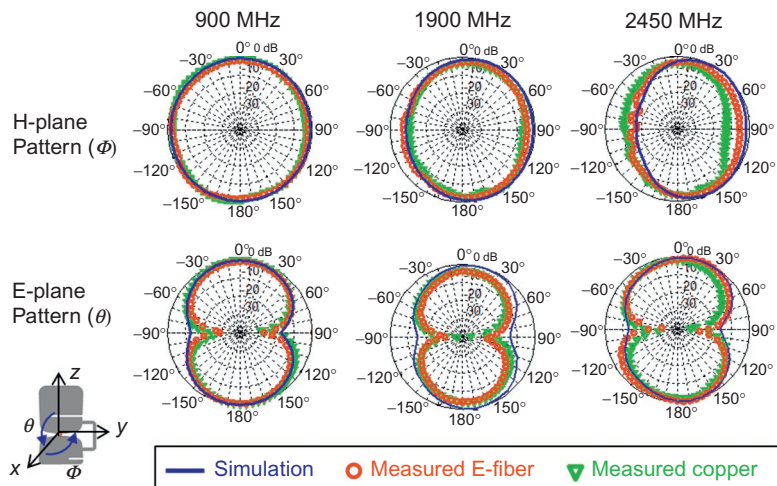


**Figure 10.23** Measured and simulated radiation pattern of the multiband textile antenna in free space.

*Detuning of resonance frequency:* To study the influence of the human body on antenna performance, a three-layer tissue substrate was placed under the antenna simulation model (Ouyang et al., 2009). As shown in Figure 10.24, the truncated three-layer tissue model was composed of 1-mm-thick skin, 3-mm-thick fat, and 40-mm-thick muscle, all of which exhibited frequency-dependent properties (Christ et al., 2006). In addition, we included an air gap between the antenna and the tissue substrate to emulate the presence of clothing (Wang et al., 2014). The simulated S11 data in Figure 10.24 show that frequency detuning of the multiband antenna is increased as the air gap reduces. To retain sufficient bandwidth at all three bands, the antenna needs to be placed at least 10 mm away from the tissue to mitigate unfavorable body effects.

*Radiation pattern shadowing:* An omnidirectional antenna cannot retain its radiation pattern due to signal blocking caused by the underlying human body. To address this issue computationally, we used a full-scale human phantom (height = 180 cm and chest width = 53 cm) (Wang et al., 2014) and evaluated the antenna on different on-body locations: front and back torso, arm, and shoulder. Figure 10.25 gives the co-polarized and cross-polarized upper-hemisphere radiation patterns of the shoulder-mounted antenna. It is obvious that the human body affects the original omnidirectional radiation patterns. In particular, the front-to-back ratios ( $\text{gain}_{\max}/\text{gain}_{\min}$ ) are higher than 15 dB.

We further considered the cross-polarized radiation of the multiband antenna, because polarization mismatch is unavoidable due to the individual's movements. As shown in Figure 10.25, the shoulder-mounted antenna still provides coverage in cross-polarization operation. This is because the antenna's surface shared the shoulder and arm sections of the body. The shoulder-mounted antenna did provide a good

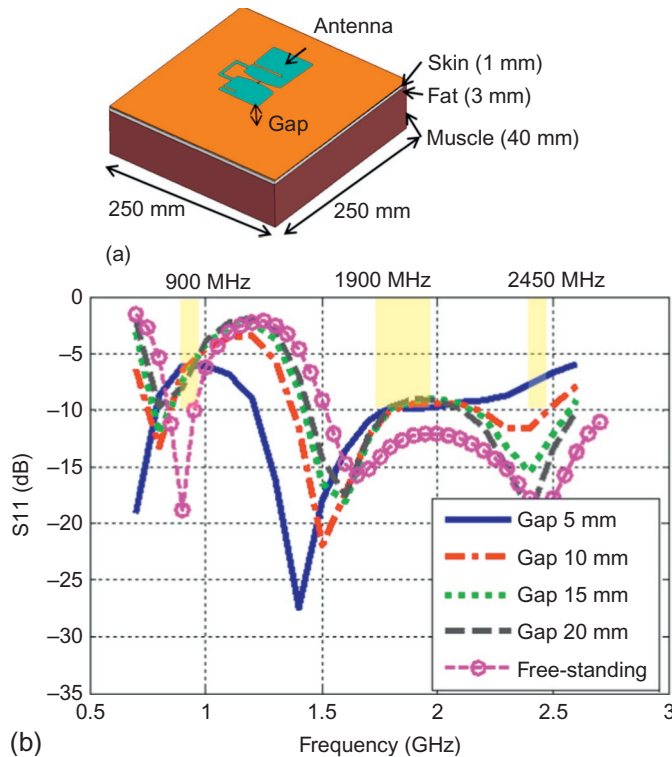


**Figure 10.24** Influence of human tissues on antenna resonance: (a) simulation model and (b) simulated  $S_{11}$  for different gap distances.

From Wang et al. (2014), ©2014 IEEE.

co-polarization pattern as well. Therefore, we can conclude that shoulder mounting is preferred for improved radiation coverage in the upper hemisphere.

### 10.5.2.3 Body-worn textile antenna for cellular communications

We next proceeded to integrate a cell phone into the proposed body-worn antenna. The goal was to replace the embedded cellular antenna with a body-worn antenna. As shown in Figure 10.26, the textile antenna was embroidered inside the shoulder pad of a jacket (provided by Peerless Clothing Inc.). Concurrently, the embedded cell phone antenna was deactivated. We did so using a Nokia 6600 cell phone, and connecting it directly to the textile antenna via a wire running through the jacket (see Figure 10.26). Therefore, the textile antenna served as the main receiving/transmitting antenna for the cell phone. With the textile antenna in use, the cell phone signal strength was evaluated indoors while the user moved around a commercial building. For simplicity, we used the cell phone's "signal bars" to estimate the quality of the received signal. We note that the number of signal bars on this phone ranged from

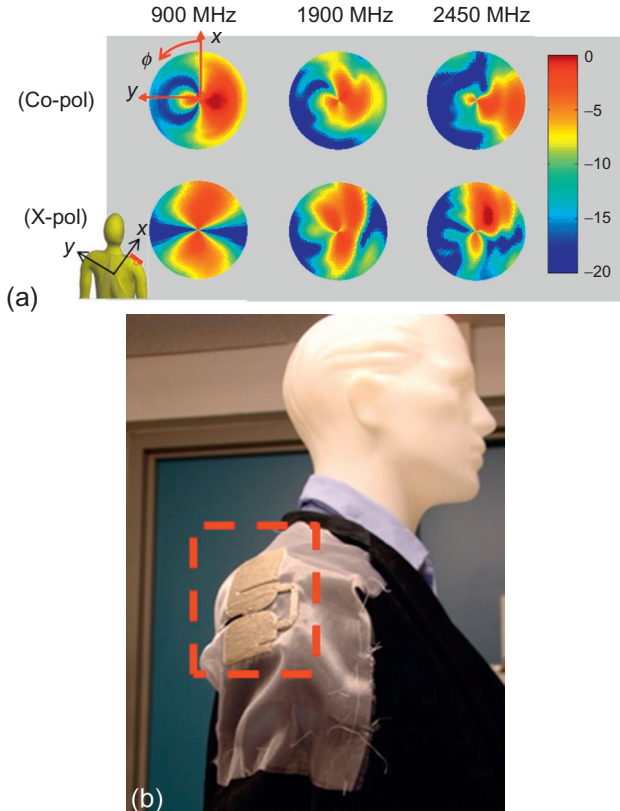


**Figure 10.25** (a) Simulated upper-hemisphere ( $\theta = 0$ – $90^\circ$ ,  $\phi = 0$ – $360^\circ$ ) projected patterns (co- and cross polarization) when the textile antenna is mounted on the phantom’s shoulder and (b) shoulder-mounted textile antenna on a phantom. Pattern plots are in dB scale.  
From Wang et al. (2014), ©2014 IEEE.

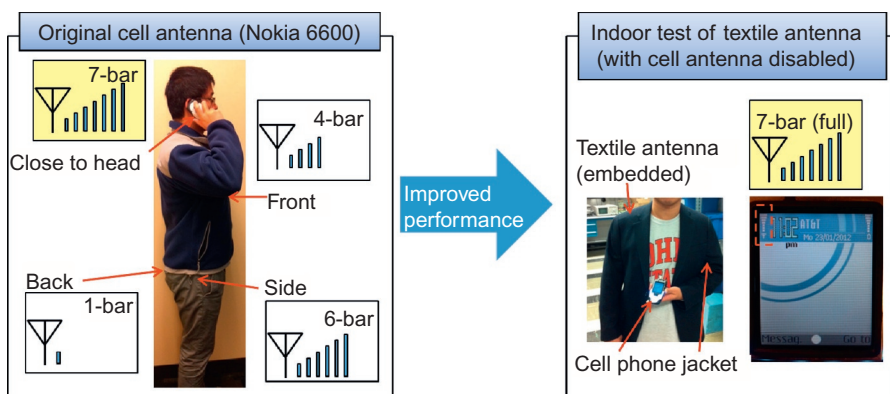


**Figure 10.26** Wearable textile antenna system for body-worn cellular communications. We note that the relationship between signal bars and actual power is as follows: “1-bar”: -100 to -95 dBm; “4-bar”: -85 to -80 dBm; “6-bar”: -75 to -70 dBm; and “7-bar”: > -70 dBm.  
From Wang et al. (2014), ©2014 IEEE.

0 to 7, with each bar representing 5 dB steps. Also, for the tested phone, the signal corresponding to 0 bar is about  $-105$  dBm to  $-100$  dBm. Figure 10.26 shows that a full-strength signal (7-bar) was consistently obtained when the cell phone was connected to the textile antenna on the shoulder. By contrast, the original cell phone antenna provided a full-strength signal only when the cell phone was held close to the head. For other phone-held locations, such as front, back, and side pockets (see Figure 10.26), the signal strength was reduced. Therefore, we remarked that the body-worn textile antenna provided a consistently strong signal. Of course, its inconspicuous mounting into the clothing adds comfort.

### **10.5.3 Embroidered ultra wideband spiral antenna for conformal applications**

Low-profile and lightweight ultra wideband antennas are advantageous for conformal RF installations. Concurrently, as demonstrated in the previous sections, embroidered conductive textiles have shown low-loss characteristics from 30 MHz to 4 GHz. Therefore, it is of interest to design ultra wideband textile antennas for conformal applications. Here, a 300–3000 MHz ultra wideband textile spiral was designed and fabricated using conductive textiles. As shown in Figure 10.27, the proposed slot spiral antenna consisted of a slotline wound in an Archimedean spiral with a diameter of  $\sim 208$  mm (8-in.). Two  $90\ \Omega$  resistors were placed at the slot ends to match the characteristic impedance of the slotline ( $\sim 100\ \Omega$ ) and minimize current reflections from the end. Meanwhile, a wideband microstrip planar balun ( $50\ \Omega$ , half that of the slotline) was directly integrated into the antenna aperture to ensure broadband feeding (see Figure 10.27). This approach provided for an extremely broadband impedance and efficient space utilization. As shown in Figure 10.27, the textile slot spiral and the microstrip textile balun were fabricated onto a 1.3-mm-thick PDMS substrate to form the spiral's aperture. To build the feeding, the textile balun was spiraled in toward the center of the antenna and connected to the slot spiral layer using E-fibers through the substrate. In practice, a 25-mm-thick shallow reflecting cavity composed of copper ground plane was employed to enforce unidirectional radiation. Importantly, due to the fact that the slot antenna was a magnetic current radiator, the cavity was placed sufficiently close to the slot, with its thickness approximately  $\lambda=40$  deep at 300 MHz (see Figure 10.28).

As shown in Figure 10.28, the fabricated textile spiral exhibited a 10:1 bandwidth, operating from 300 MHz to 3 GHz. It also delivered a consistent circularly polarized gain of 5 dBi, except at the lower and higher ends of the frequency band. At low frequencies, the resistive termination decreased the antenna efficiency. Conversely, at higher frequencies, coupling between the microstrip balun and the slot spiral degraded the realized gain. The measured patterns were shown to be uniform across the wide band and matched well with the simulated results (see Figure 10.28). This pattern uniformity also indicated that the load termination for this spiral microstrip balun functioned properly over the entire band.

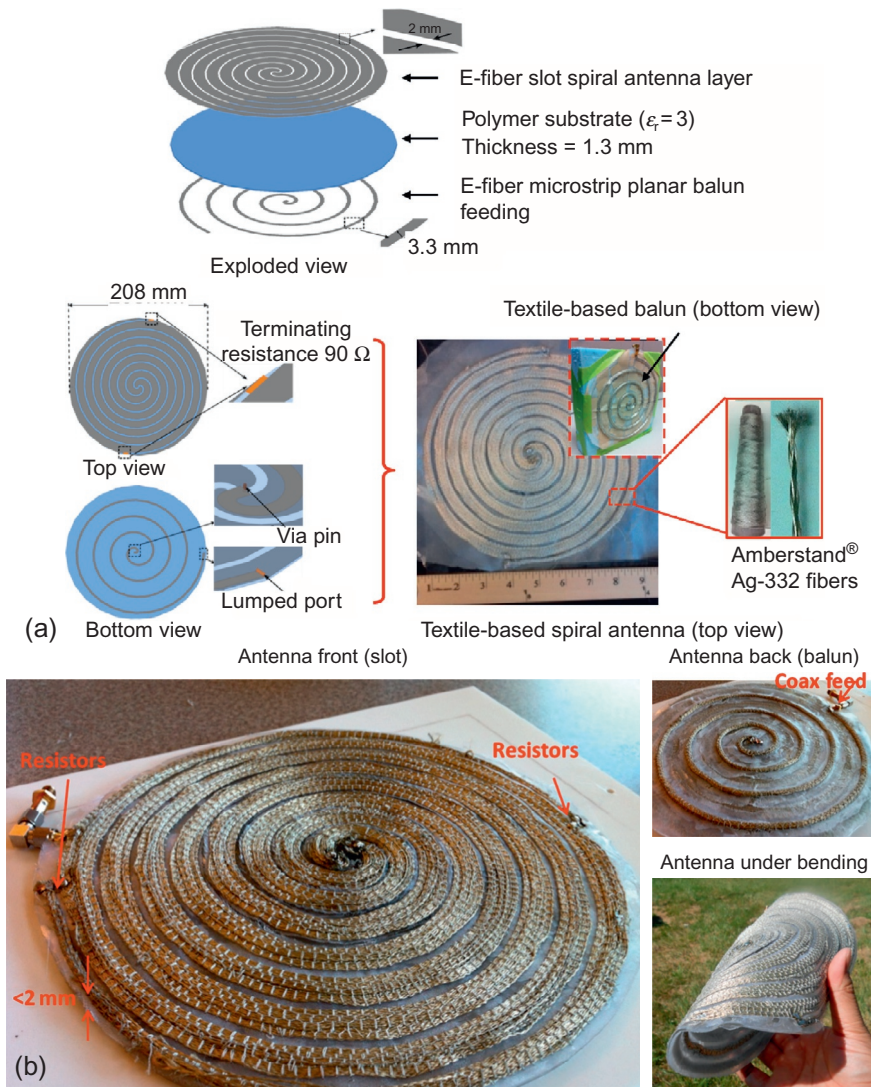


**Figure 10.27** Design of an 8-in. textile slot spiral with a self-contained microstrip planar balun: (a) design model and (b) fabricated sample.

From [Wang et al. \(2013b\)](#), ©2013 IEEE.

#### 10.5.4 Embroidered textile lung sensor for health care monitoring

In this section, we focus on the design and characterization of an RF textile sensor that can be used for monitoring lung fluids, a precursor to congestive heart failure. As demonstrated in [Salman et al. \(2014\)](#), experimental validation of this RF sensor is carried out on a human phantom filled with a fresh porcine lung. Concurrently, we also

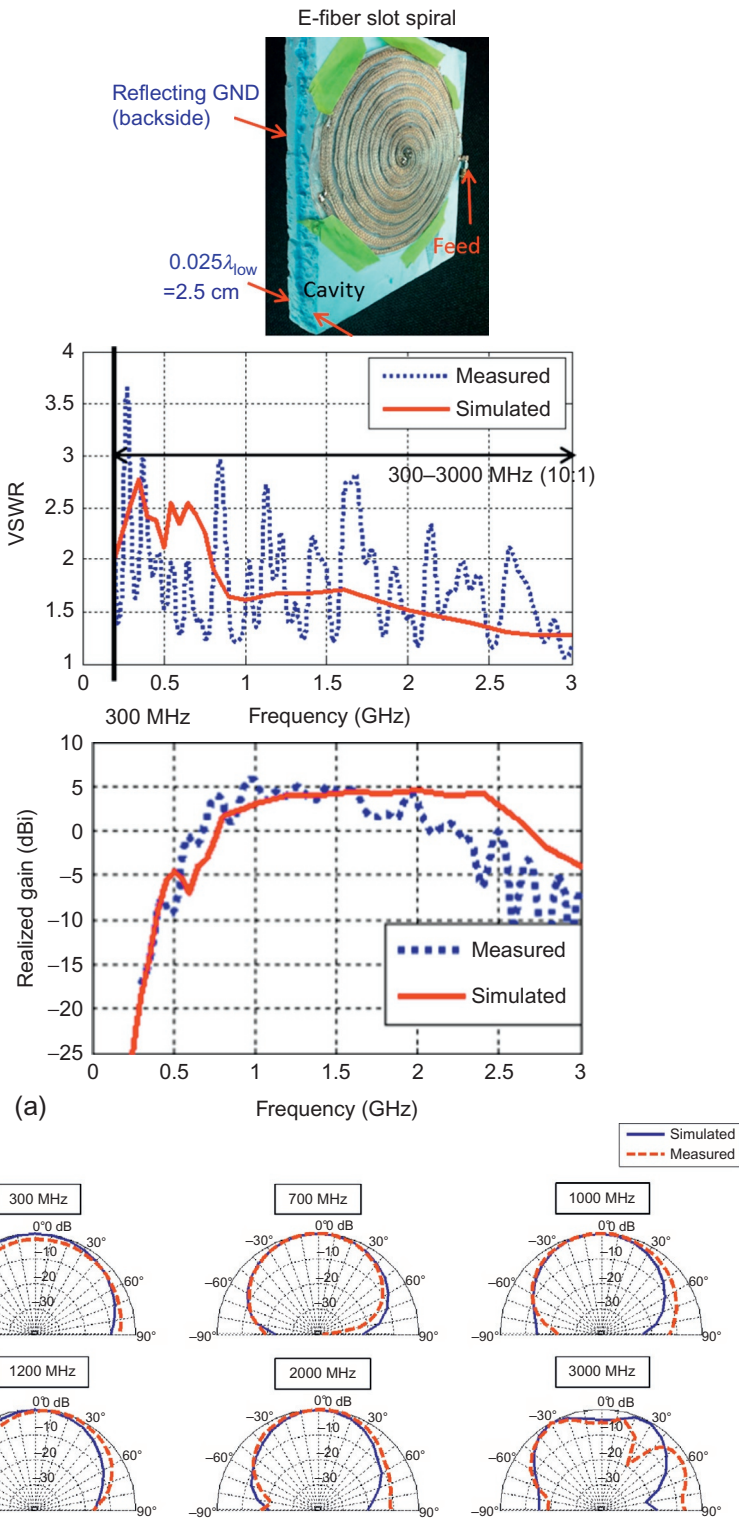


**Figure 10.28** Textile slot spiral with shallow reflecting cavity: (a) measured voltage standing wave ratio (VSWR) and circularly polarized gain and (b) measured radiation pattern across the band.

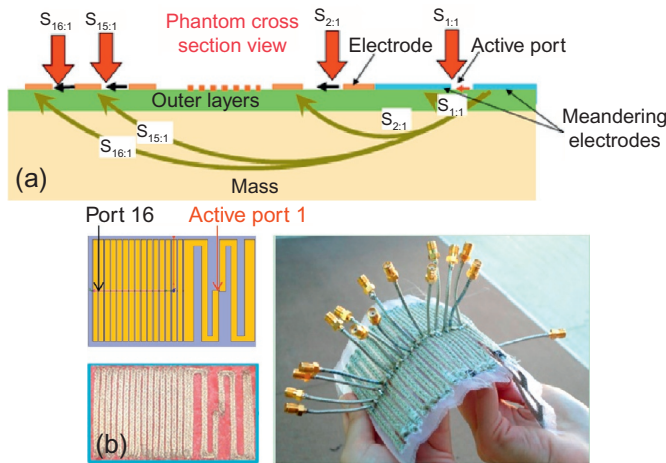


**Figure 10.29** (a) Operation principle of the lung sensor and (b) the designed and fabricated textile sensor.

Panel (a): From [Salman et al. \(2014\)](#), ©2014 IEEE. Panel (b): From [Zhang et al. \(2012\)](#), ©2012 IEEE.

developed a body-area network for medical sensing (MS-BAN) integrated with the RF sensor for continuous remote monitoring ([Salman et al., 2014](#)).

Because the sensor's penetration depth is proportional to its size, sensors of large surface area can penetrate deeper into the body. In this regard, the proposed embroidered E-fiber technology is suitable to fabricate large-size textile sensors that can be inconspicuously integrated as part of the garment on various locations (front, back, shoulders, etc.). The designed sensor consists of one excitation port (port 1) and 15 receiving electrodes (length = 0 cm, width = 1 cm; see [Figure 10.29](#)). As shown in [Figure 10.29](#), the fields propagate from the excitation port (port 1) to the other ports. The port voltages are subsequently measured and postprocessed to obtain the lung's dielectric constant ([Salman et al., 2014](#)).

As illustrated in [Figure 10.30](#), both textile and metallic (copper) sensors are fabricated. Their sensing performance was tested by evaluating the S-parameters of the sensor placed upon ground beef, at 40 MHz ([Zhang et al., 2012](#)). It is seen that the measured S-parameters from the textile sensor are in good agreement with those of its copper counterpart. The discrepancies observed at ports 9, 11, and 14 are primarily due to inaccuracies in the fabricated textile sensor. Regardless, these measurements imply that the textile sensor is equally effective to its copper counterpart.

### 10.5.5 Embroidered RFID antennas for tire-tracking applications

With the increasing demand for automated inventory tracking and item identification, passive UHF RFID systems have been extensively adapted. As shown in [Figure 10.31](#), an important application is to integrate these RFID tags into commercial truck tires to

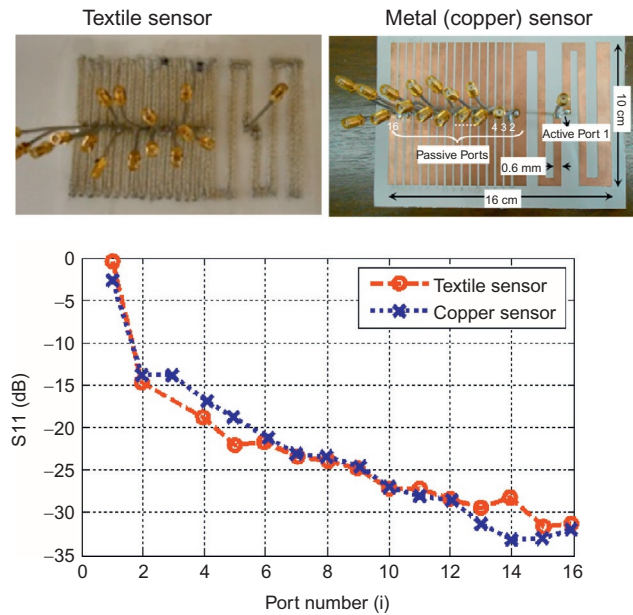


**Figure 10.30** Comparison between the measured S-parameters of textile and copper sensors. From [Zhang et al. \(2012\)](#), ©2012 IEEE.

monitor the tires' health condition ([Shao et al., 2014a](#)). However, RFID tags integrated into a tire endure frequent changes in pressure, stress, temperature, and permittivity of the surrounding rubber ([Shao et al., 2014a,b](#)). Therefore, the tag antennas must be structurally tough and flexible to endure such changes.

As discussed in [Shao et al. \(2014a,b\)](#), conventional metallic RFID tag antennas are not flexible and stretchable, and even the metal wire can eventually fail from metal fatigue. Thus, metallic antennas may get structurally deformed when operating inside a tire environment. This, in turn, detunes the antennas and reduces the read range of the tag (see [Figure 10.31a](#)). As an alternative, textile antennas integrated into stretchy polymer have been proposed. The latter exhibit significant mechanical flexibility, stretchability, and durability and demonstrate excellent RF performance, comparable to that of their copper counterparts. Additionally, the polymer coating ([Wang et al., 2012b](#)) maintains the mechanical integrity of the tag and facilitates its integration into the tire sidewall.

For example, [Figure 10.32](#) shows two embroidered RFID tag antennas: (a) a folded dipole textile antenna ([Shao et al., 2014a](#)) and (b) an end-loaded meander-line (ELML) textile antenna ([Shao et al., 2014b](#)). The antennas are further connected to RFID chips for tire-sensing applications. The RF performance of these embroidered RFID textile antennas is evaluated by conducting reader threshold power tests at a fixed distance ([Shao et al., 2014a](#)). Of course, a lower threshold power indicates a longer read range. The textile antennas are tested on a rubber sample ( $\epsilon_r = 3.66$ ) obtained

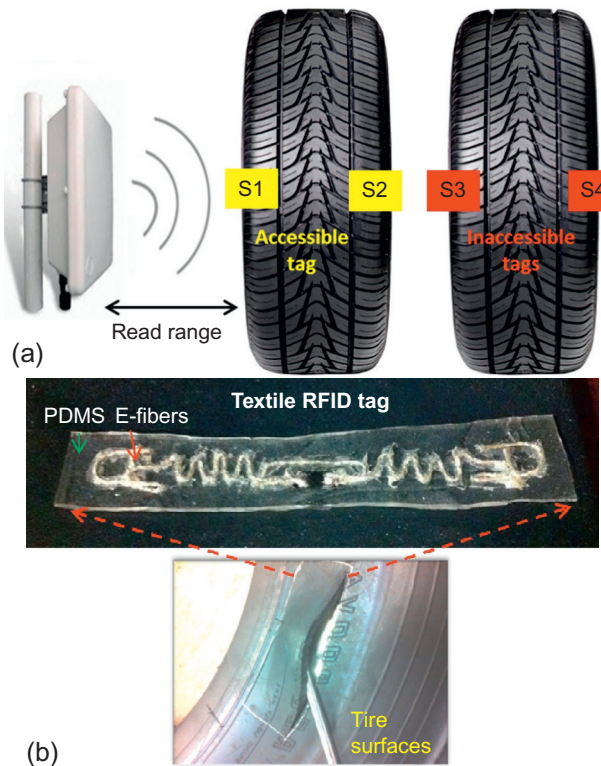


**Figure 10.31** (a) Tires on dual-wheel situation: existing tags cannot be detected when mounted on sidewall S3 and S4 of the inner tire and (b) embroidered textile RFID tag embedded inside the truck tire.

From [Shao et al. \(2014a\)](#), ©2014 IEEE.

**Table 10.4 Threshold power test of embroidered RFID textile antenna**

Antenna material	Folded dipole textile antenna ( <a href="#">Shao et al., 2014a</a> )		ELML antenna ( <a href="#">Shao et al., 2014b</a> )	
	Copper	Embroidered textile	Copper	Embroidered textile
Reader threshold power	22 dBm	24 dBm	20 dBm	22 dBm

[Shao et al. \(2014a,b\).](#)

from an actual truck tire ([Shao et al., 2014a](#)) and further compared with their copper wire counterparts. As shown in **Table 10.4**, the measured threshold power of both embroidered RFID antennas is as good as that of their copper wire counterparts, only 2 dB higher. Thus, we remark that the embroidered RFID textile antennas provide

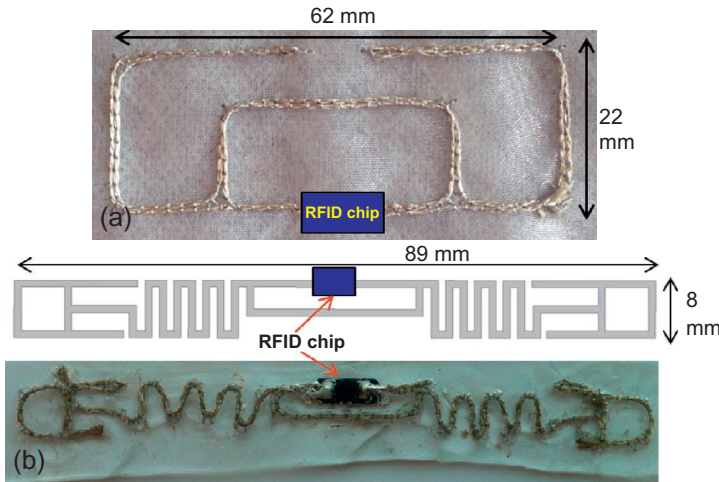


**Figure 10.32** (a) Tires on dual-wheel situation: existing tags cannot be detected when mounted on sidewall S3 and S4 of the inner tire and (b) embroidered textile RFID tag embedded inside the truck tire.

From Shao et al. (2014a, 2014b), ©2014 IEEE.

excellent RF performance, comparable to that of their conventional metallic counterparts, in addition to their inherent mechanical flexibility, stretchability, and durability (Shao et al., 2014a,b).

## 10.6 Conclusion

This chapter presented a novel class of embroidered textile antennas and RF circuits based on electrically conductive metal-polymer fibers (E-fibers). These textile-based RF circuits and antennas are developed to realize wearable RF electronics woven into daily garments. The proposed E-fibers are composed of a high-strength and flexible polymer core (10 µm thick) covered with a metallic coating (2 µm thick). These E-fibers exhibit very low electrical loss and excellent mechanical strength and flexibility. Computerized embroidery and high-density stitching are used to achieve high conductivity and accurate fabrication of the E-fiber textile surfaces woven into regular clothing. Using this process, prototype textile antennas and RF circuits are fabricated and tested. The measured results demonstrated that the embroidered textile antennas' RF performance is nearly as good as that of conventional copper antennas, namely, less than 1 dB lower. This is in addition to their excellent mechanical strength and flexibility. Importantly, the textile antennas can be inconspicuously woven into clothing, without affecting comfort, fashionably, and washability. Consequently, a variety of textile-based flexible and wearable antennas and sensors were designed and

measured for wireless communications, medical sensing, and RFIDs. Overall, the proposed embroidered textile antennas and RF circuitries provide solutions to future RF functionalized and fashionable garments for wearable high-speed communications with omnidirectional coverage.

## 10.7 Future work

Our work to date on electrically conductive fibers (E-fibers) has demonstrated reliable fabrication and excellent performance of the embroidered antennas and circuits (Wang et al., 2012b, 2013a). Nevertheless, a challenge that needs to be addressed in the future is the improvement of the embroidery's geometrical accuracy, without degrading the conductivity of the textile surfaces. Thicker E-fibers are more conductive, and have the potential to increase the effective conductivity of the embroidered surface to the point where it behaves much like a conductor. However, use of thick E-fibers is inconsistent with the requirement for high geometrical accuracy in embroidery. This, in contrast, requires thin and fine conductive yarns. We note that our current technology employs E-fibers of 0.5 mm in diameter (664 tightly bundled strands), and applies double-layer stitching at a density of 2.0 lines/mm (Wang et al., 2012b). In this case, the RF performance of the textile prototypes is comparable to that of copper, while the accuracy in embroidering details is of the order of 1 mm.

Aiming for a complete E-fiber replacement of copper, a goal for the future is to further improve the aforementioned embroidery technology so as to achieve an accuracy of as good as 0.1 mm, without degrading conductivity. The idea is to employ thinner E-fibers, which exhibit low embroidery tension and high flexibility, and can therefore print very accurately. For example, Figure 10.33 indicates how thinner E-fibers are more accurate in (a) printing fine details and (b) achieving sharp, clean corners. E-fibers of 664 down to 20 strands will be tested in the future. Another

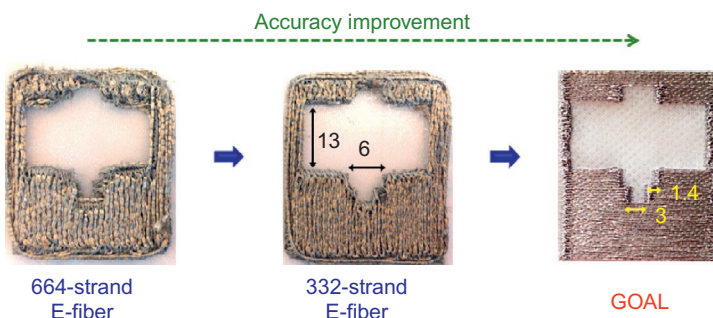


**Figure 10.33** Improvement in embroidery accuracy by employing thinner E-fibers. Dimensions shown are in mm.

challenge in this case is to optimize the ply thickness, thread weight, and twisting/braiding angles of the E-fibers.

To account for the resulting trade-off in conductivity due to the use of thin E-fibers, the stitching patterns will need to be modified accordingly. The goal is to minimize physical discontinuities and increase the conductivity of the embroidered surfaces. For this purpose, denser ( $>2.0$  lines/mm) and multilayer ( $>2$  layers) embroidery will be employed, as indicated in [Figure 10.34](#). A challenge in this case is to avoid sewing needle breakage from mechanical fatigue. Another challenge is that the top E-fiber layers that will be stitched upon the “stiff” underlying E-fiber layers might slightly lose alignment.

Concurrently, further work will be performed in the future to fulfill application-specific requirements for conductive embroidered structures. For example, wearable textile antennas should be flexible and resilient to repetitive washing, while looking and feeling like regular fabric ([Wang et al., 2013a](#)). Textile antennas for aerial applications should be mechanically strong and conformal ([Wang et al., 2013b](#)). Textile RFID antennas for automotive tire sensing should be stretchable to an additional 10–20% beyond their normal size ([Shao et al., 2014a,b](#)). Research areas that aim to address such requirements include (1) integration of E-fiber structures into stretchy polymer; (2) embroidery on novel, lightweight, high-strength, and stable fabrics (Kevlar, felt, etc.); and (3) evaluation of textile prototypes under mechanical (tensile/shear/flexure/vibration) stresses and temperature variations.

Given their extreme flexibility and the impressive results to date, E-fibers have the potential to revolutionize RF communications. Further refining the embroidery accuracy and addressing the per-case requirements for flexibility, stretchability, strength,

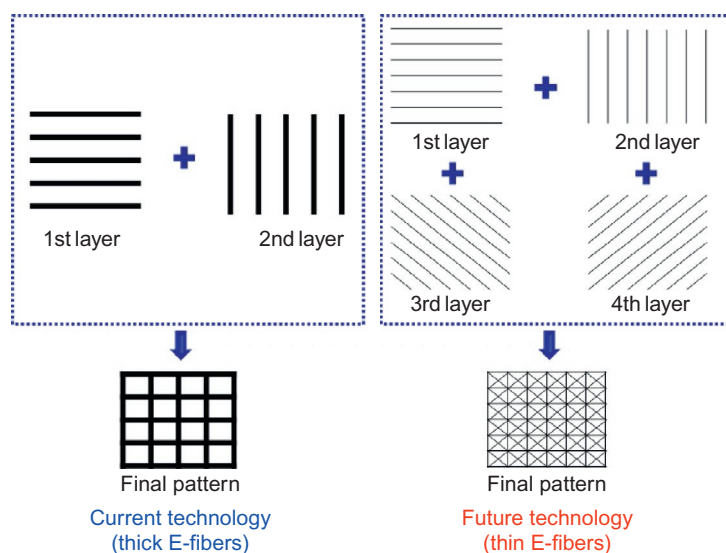


**Figure 10.34** Denser stitching patterns for thin E-fibers to achieve highly conductive textile surfaces.

and more will help establish the use of conductive textiles in a great deal of industries, including health care, leisure, sports, consumer electronics, military/defense, aerospace, and others.

## References

- Bashir, S., Chauraya, A., Edwards, R.M., Vardaxoglou, J., 2009. A flexible fabric meta-surface for on body communication applications. In: Presented at Loughborough Antennas Propagation Conference, Loughborough, UK. <http://dx.doi.org/10.1109/LAPC.2009.5352436>.
- Christ, A., Klingensbock, A., Samaras, T., Goiceanu, C., Kuster, N., 2006. The dependence of electromagnetic far-field absorption on body tissue composition in the frequency range from 300 MHz to 6 GHz. *IEEE Trans. Microw. Theory. Tech.* 54 (5), 2188–2195. <http://dx.doi.org/10.1109/TMTT.2006.872789>.
- Chung, J.Y., Nahar, N.K., Zhang, L., Bayram, Y., Sertel, K., Volakis, J.L., 2012. Broadband RF conductivity measurement technique for engineered composites. *IET Microw. Antennas Propag.* 6 (4), 371–376. <http://dx.doi.org/10.1049/iet-map.2011.0349>.
- Hamed, M., Forchheimer, R., Inganas, O., 2007. Towards woven logic from organic electronic fibres. *Nat. Mater.* 6 (5), 357–362. <http://dx.doi.org/10.1038/nmat1884>.
- Kim, G., Lee, J., Lee, K.H., Chung, Y.C., Yeo, J., Moon, B.H., Yang, J., Kim, H.C., 2008. Design of a UHF RFID fiber tag antenna with electric-thread using a sewing machine. In: Presented at the Asia-Pacific Microwave Conference, Macau, China. <http://dx.doi.org/10.1109/APMC.2008.4958396>.
- Koulouridis, S., Kizitas, G., Zhou, Y., Hansford, D.J., Volakis, J.L., 2006. Polymer-ceramic composites for microwave applications: fabrication and performance assessment. *IEEE Trans. Microw. Theory. Tech.* 54 (12), 4202–4208. <http://dx.doi.org/10.1109/TMTT.2006.885887>.
- Lee, G.Y., Psychoudakis, D., Chen, C.C., Volakis, J.L., 2011. Channel decomposition method for designing body-worn antenna diversity system. *IEEE Trans. Antennas Propag.* 59 (1), 254–262. <http://dx.doi.org/10.1109/TAP.2010.2078444>.
- Li, Y., Torah, R., Beeby, S., Tudor, J., 2012. An all-inkjet printed flexible capacitor on a textile using a new poly (4-vinylphenol) dielectric ink for wearable applications. In: IEEE Sensors. pp. 1–4. <http://dx.doi.org/10.1109/ICSENS.2012.6411117>.
- Lilja, J., Salonen, P., Kaija, T., Maagt, P.D., 2012. Design and manufacturing of robust textile antennas for harsh environments. *IEEE Trans. Antennas Propag.* 60 (9), 4130–4140. <http://dx.doi.org/10.1109/TAP.2012.2207035>.
- Locher, I., Troster, G., 2008. Enabling technologies for electrical circuits on a woven monofilament hybrid fabric. *Text. Res. J.* 78 (7), 583–594. <http://dx.doi.org/10.1177/0040517507081314>.
- Mangan, A.M., Voinigescu, S.P., Yang, M.T., Tazlauanu, M., 2006. De-embedding transmission line measurements for accurate modeling of IC designs. *IEEE Trans. Electron. Devices* 53 (2), 235–241. <http://dx.doi.org/10.1109/TED.2005.861726>.
- Mehdipour, A., Sebak, A.R., Trueman, C.W., Rosca, I.D., Hoa, S.V., 2010. Reinforced continuous carbon-fiber composites using multi-wall carbon nanotubes for wideband antenna applications. *IEEE Trans. Antennas Propag.* 58 (7), 2451–2456. <http://dx.doi.org/10.1109/TAP.2010.2048862>.
- Morris, S.E., Bayram, Y., Zhang, L., Wang, Z., Shtein, M., Volakis, J.L., 2011. High-strength, metalized fibers for conformal load bearing antenna applications. *IEEE Trans. Antennas Propag.* 59 (9), 3458–3462. <http://dx.doi.org/10.1109/TAP.2011.2161442>.

- Ouyang, Y., Chappell, W.J., 2008. High frequency properties of electro-textiles for wearable antenna applications. *IEEE Trans. Antennas Propag.* 56 (2), 381–389.
- Ouyang, Y., Love, D.J., Chappell, W.J., 2009. Body-worn distributed MIMO system. *IEEE Trans. Veh. Technol.* 58 (4), 1752–1765. <http://dx.doi.org/10.1109/TAP.2007.915435>.
- Pozar, D., 2004. *Microwave Engineering*. John Wiley & Sons Inc., New York.
- Salman, S., Wang, Z., Colebeck, E., Kiourti, A., Topsakal, E., Volakis, J.L., 2014. Pulmonary edema monitoring sensor with integrated body-area network for remote medical sensing. *IEEE Trans. Antennas Propag.* 62 (5), 2787–2794. <http://dx.doi.org/10.1109/TAP.2014.2309132>.
- Shao, S., Kiourti, A., Burkholder, R., Volakis, J.L., 2014a. Flexible and stretchable UHF RFID tag antennas for automotive tire sensing. In: Presented at the European Conference on Antennas and Propagation, Hague, The Netherlands. <http://dx.doi.org/10.1109/EuCAP.2014.6902434>.
- Shao, S., Kiourti, A., Burkholder, R., Volakis, J.L., 2014b. Broadband and flexible textile RFID tags for tires. In: Presented at IEEE International Symposium on Antennas and Propagation, Memphis, Tennessee. <http://dx.doi.org/10.1109/APS.2014.6905079>.
- Toyobo Co., Ltd, 2005. PBO Fibers Zylon Technical Information. Available from: [www.toyobo-global.com/seihin/kc/pbo](http://www.toyobo-global.com/seihin/kc/pbo).
- Vallozzi, L., Rogier, H., Hertleer, C., 2009. A textile patch antenna with dual polarization for rescue workers' garments. In: Presented at European Conference on Antennas Propagation, Berlin, Germany.
- Volakis, J.L., Zhang, L., Wang, Z., Bayram, Y., 2012. Embroidered flexible RF electronics. In: Presented at the IEEE International Workshop on Antenna Technology, Tucson, Arizona. <http://dx.doi.org/10.1109/IWAT.2012.6178385>.
- Wang, Z., Zhang, L., Psychoudakis, D., Volakis, J.L., 2012a. Flexible textile antennas for body-worn communications. In: Presented at the IEEE International Workshop on Antenna Technology, Tucson, Arizona. <http://dx.doi.org/10.1109/IWAT.2012.6178647>.
- Wang, Z., Zhang, L., Bayram, Y., Volakis, J.L., 2012b. Embroidered conductive fibers on polymer composite for conformal antennas. *IEEE Trans. Antennas Propag.* 60 (9), 4141–4147. <http://dx.doi.org/10.1109/TAP.2012.2207055>.
- Wang, Z., Zhang, L., Volakis, J.L., 2013a. Textiles antennas for wearable radio frequency applications. *J. Text. Light Ind. Sci. Technol.* 2 (3), 105–112.
- Wang, Z., Lee, L.Z., Volakis, J.L., 2013b. A 10:1 bandwidth textile-based conformal spiral antenna with integrated planar balun. In: Presented at the IEEE International Symposium on Antennas and Propagation, Orlando, Florida. <http://dx.doi.org/10.1109/APS.2013.6710771>.
- Wang, Z., Lee, L.Z., Psychoudakis, D., Volakis, J.L., 2014. Embroidered multiband body-worn antenna for GSM/PCS/WLAN communications. *IEEE Trans. Antennas Propag.* 62 (6), 3321–3329. <http://dx.doi.org/10.1109/TAP.2014.2314311>.
- Zhang, L., Wang, Z., Volakis, J.L., 2012. Textiles antennas and sensors for body-worn applications. *IEEE Antennas Wirel. Propag. Lett.* 11, 1690–1693. <http://dx.doi.org/10.1109/LAWP.2013.2239956>.
- Zhou, Y., Bayram, Y., Du, F., Dai, L., Volakis, J.L., 2010. Polymer-carbon nanotube sheet for conformal load bearing antennas. *IEEE Trans. Antennas Propag.* 58 (7), 2169–2175. <http://dx.doi.org/10.1109/TAP.2010.2048852>.